Tectonophysics 789 (2020) 228481

Contents lists available at ScienceDirect

Tectonophysics

journal homepage: www.elsevier.com/locate/tecto

Tectonics and seismicity in the Northern Apennines driven by slab retreat and lithospheric delamination

M. D'Acquisto[a,b,*], L. Dal Zilio[a,c], I. Molinari[a,d], E. Kissling[a], T. Gerya[a], Y. van Dinther[a,b]

[a] Department of Earth Sciences, ETH Zürich, Sonneggstrasse 5, Zürich, Switzerland
[b] Department of Earth Sciences, Utrecht University, Princetonlaan 8A/4, Utrecht, Netherlands
[c] Division of Geological and Planetary Science, California Institute of Technology, 1200 E California Blvd, Pasadena, USA
[d] Sezione di Bologna, Istituto Nazionale di Geofisica e Vulcanologia, via Donato Creti 12, Bologna, Italy

ARTICLE INFO

Keywords:
Numerical modeling
Geodynamics
Seismotectonics orogen
Delamination
Northern Apennines

ABSTRACT

Understanding how long-term subduction dynamics relates to the short-term seismicity and crustal tec tonics is a challenging but crucial topic in seismotectonics. We attempt to address this issue by linking long-term geodynamic evolution with short-term seismogenic deformation in the Northern Apennines. This retreating subduction orogen displays tectonic and seismogenic behaviors on various spatiotemporal scales that also characterize other subduction zones in the Mediterranean area. We use visco-elasto-plastic seismo-thermo-mechanical (STM) modeling with a realistic 2D setup based on available geological and geophysical data. The subduction dynamics and seismicity are coupled in the numerical modeling, and driven only by buoyancy forces, i.e., slab pull. Our results suggest that lower crustal rheology and lithospheric mantle temperature modulate the crustal tectonics of the Northern Apennines, as inferred by previous studies. The observed spatial distribution of upper crustal tectonic regimes and surface displacements requires buoyant, highly ductile material in the subduction channel beneath the internal part of the orogen. This allows protrusion of the asthenosphere in the lower crust and lithospheric delamination associated with slab retreat. The resulting surface velocities and principal stress axes generally agree with present-day observations, suggesting that slab delamination and retreat can explain the dynamics of the orogen. Our simulations successfully reproduce the type and overall distribution of seismicity with thrust faulting events in the external part of the orogen and normal faulting in its internal part. Slab temperatures and lithospheric mantle stiffness affect the cumulative seismic moment release and spatial distribution of upper crustal earthquakes. The properties of deep, sub-crustal material are thus shown to influence upper crustal seismicity in an orogen driven by slab retreat, even though the upper crust is largely decoupled from the lithospheric mantle. Our simulations therefore highlight the effect of deep lower crustal rheologies, self-driven subduction dynamics and mantle properties in controlling shallow deformation and seismicity.

1. Introduction

The geodynamic evolution and seismicity of many orogenic systems in the Mediterranean domain, such as the Apennines, Carpathians, Hellenides or the Betic-Rif systems, are driven by the rapid Cenozoic retreat of genetically associated slabs (e.g., Vergés and Fernàndez, 2012; van Hinsbergen et al., 2014; Faccenna et al., 2013, 2014a, 2014b; Horváth et al., 2015; Balázs et al., 2017; Jolivet and Brun, 2010; Jolivet et al., 2013). The evolution of such an orogen is typically characterized by the gradual migration towards the foreland of contraction in the external part and extension in the internal part, driven by slab retreat (Bertotti et al., 2006; Picotti and Pazzaglia, 2008; Leever et al., 2006). The extension is defined as back-arc, although often there is no stable magmatic arc observed (see discussion in Jolivet et al., 2013). Numerous reconstructions, geodynamic modeling studies of subduction dynamics and magmatism, as well as extensive analysis of present-day seismicity and surface to deep mantle observations are readily available in the entire Mediterranean (e.g., Funiciello et al., 2006; Menant et al., 2016; Spakman et al., 2018; Andrić et al., 2018; Serpelloni et al., 2013; Métois et al., 2015; Faccenna et al., 2014a; Konstantinou, 2017; van Hinsbergen et al., 2020; Király et al., 2018). However, the multi-scale quantitative coupling between long-term geodynamic evolution and short-term seismogenic deformation is more poorly understood. We analyze this interplay in one well-known example of such a typical retreating subduction orogen, the Northern Apennines (Fig. 1). Particularly, we aim to better understand the impact of deep processes and

* Corresponding author at: Department of Earth Sciences, Utrecht University, Princetonlaan 8A, Utrecht, Netherlands.
E-mail address: m.dacquisto@uu.nl (M. D'Acquisto).

https://doi.org/10.1016/j.tecto.2020.228481
Received 10 January 2020; Received in revised form 15 May 2020; Accepted 19 May 2020
Available online 30 May 2020

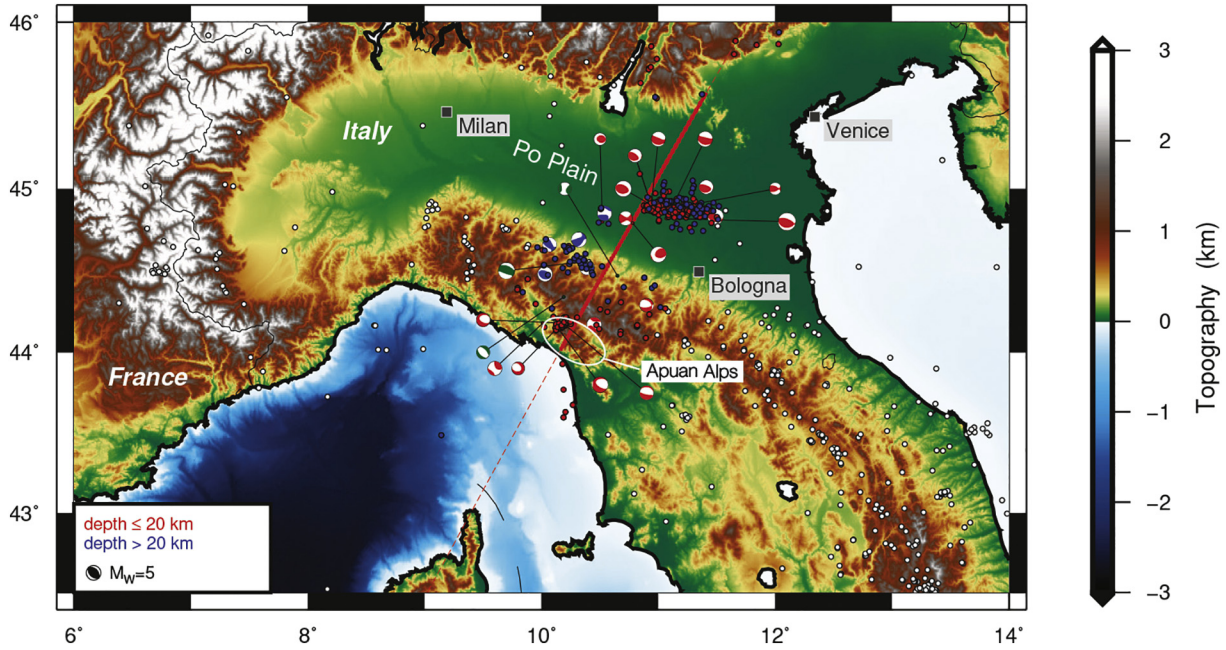

Fig. 1. Topographic map of the northern Apennines and surroundings, showing the trace of the reference profile (thick line) and its continuation (thin, dashed), as well as earthquake locations and select focal mechanisms within 25 km of the profile. The cluster of thrust-faulting events to the northeast of the Apennines consists largely of the 2012 Emilia-Romagna sequence, which activated the most external thrusts of the orogenic belt. The radius of the focal mechanisms shown scales linearly with magnitude. Hypocenter locations with no mechanism were determined by Chiarabba et al. (Chiarabba et al., 2014) on the basis of INGV recordings of earthquakes occurred between 28 February 2005 and 31 December 2014. Focal mechanisms are from an updated version (covering from 1977 to 2015) of a compilation of CMT solutions in the Italian region (Pondrelli et al., 2006).

rheologies on the seismicity typically observed at shallow upper crustal levels. The present-day expression of Apennines orogenic processes and associated seismicity results from the large scale roll-back of its genetically associated slab (i.e., the Calabrian and its northern prolongation), starting ~30 Ma. This migration of subduction was associated with compression in the external thrust belt and with gradual back-arc extension, which formed the Liguro-Provençal and Tyrrhenian basins through rotational kinematics in the overall Western Mediterranean system (Faccenna et al., 2014a; Jolivet et al., 2020; Le Breton et al., 2017, and references within). Lithospheric delamination has been invoked as the main deformation mechanism driving the tectonics and seismicity of the Northern Apennines, specifically (Chiarabba et al., 2014; Benoit et al., 2011; Panza et al., 2007). Therefore, the local buoyancy structure and lithospheric ductility could play a crucial role in the dynamics of this orogen, which might be explained by internal driving forces and rheological structure (e.g., Patacca et al., 1990; Faccenna et al., 1997, 2001; Jolivet and Faccenna, 2000; Carminati et al., 2012; Faccenna et al., 2014b; Le Breton et al., 2017; Jolivet et al., 2020).

Presently, two opposing tectonic regimes can be observed in the Northern Apennines. The frontal area is an active thrust belt with tectonic convergence at a rate of 2–3 mm yr^{-1} (Bennett et al., 2012). Most of it is subsiding at rates of ~4–5 mm yr^{-1} (but locally as fast as 9 mm yr^{-1}) and is buried by the foreland basin sediments of the Po Plain (e.g. Devoti et al., 2008; Picotti and Pazzaglia, 2008; Devoti et al., 2011; Serpelloni et al., 2013). The subsurface of the Po plain is affected by compressional earthquakes at depths of up to 20 km. Thrust-related seismicity also occurs at 20–35 km depth beneath the most external, northeastern part of the range (Chiarabba et al., 2005). To the south and west, more internally in the mountains, the thrusts are cross-cut by normal faults (Collettini et al., 2006), formed in response to the more internal extension (with ~2–3 mm yr^{-1} of horizontal motion) and modest uplift (up to ~1 mm yr^{-1}) (Bennett et al., 2012; Devoti et al., 2011; Serpelloni et al., 2013). Uplift and erosion in the most internal part of the range (in the Apuan Alps) have exhumed crustal material at an average rate of ~0.7 mm yr^{-1} since 11 Ma, with a peak of 1.3–1.8 mm yr^{-1} in the Messinian and Early Pliocene (Balestrieri et al., 2003). Uplift of what is now the crest of the chain began after the peak in exhumation of the Apuan Alps, further to the southwest, and progressed during the Pleistocene (Bartolini, 2003).

The tectonics and seismicity of the area have been the subject of renewed interest following the 2012 Emilia-Romagna earthquakes (Fig. 1). That seismic sequence activated part of the external thrust front complex through two main shocks of M_w 5.9 and 5.7, respectively (Scognamiglio et al., 2012). Historical seismicity includes several earthquakes similarly located on blind thrusts beneath the plain and at the base of the mountain range, with a maximum estimated M_w of 6.1. The middle and external parts of the range, further to the southwest, are also seismically active with earthquakes on shallow normal faults and extensionally reactivated thrusts. Among these events is the largest known earthquake in the area, the M_w ~ 6.5 Lunigiana-Garfagnana earthquake of 1920 (Rovida et al., 2016).

Despite recent studies on earthquake source mechanisms, surface deformation, and active structures in the Apennines belt (e.g., Tizzani et al., 2013; Cheloni et al., 2016), it is difficult to obtain a full picture of the seismicity and tectonics of the area and its relationship with the deep structure and geodynamics of the orogen. This is due to the limited temporal coverage of any catalog of historical and, even more so, instrumentally recorded seismicity. In the Northern Apennines, the problem is exacerbated by relatively low strain rates (~10^{-6} yr^{-1}, Chiaraluce et al., 2005) and resulting relatively low magnitudes ($M_w \leq 6.5$, Rovida et al. (2016)) and relatively long (> 160 yr) recurrence time of the largest earthquakes (Mantovani et al., 2015a). The reasonably well-known internal structure and surface observations of active deformation of the Northern Apennines can be a starting point to shed light onto the long-term dynamics and large-scale structure and its influence on tectonics and short-term seismicity.

The link between lithospheric–scale structure and geodynamics and the resulting crustal tectonics has already been the subject of global observational studies. For instance, maximum earthquake size in

subduction zones was suggested to correlate with convergence rate and lithospheric age (and thus temperature and slab pull) (e.g., Ruff and Kanamori, 1980). Furthermore, greater coupling between the slab and the rest of the subducting plate at the ocean floor was observed to correspond to less seismic moment release (Bilek et al., 2005). This is thought to reflect the effect of strength and structural integrity of the subducting plate on the localization of seismogenic brittle deformation. However, statistical correlations are often weak (e.g., Heuret et al., 2011). Furthermore, such studies are often limited by the short observational period compared to the recurrence times of earthquakes and by the difficulty of studying systems governed by multiple, interacting processes occurring at depths of tens to hundreds of kilometers and across various spatio-temporal scales. Modeling is thus needed to reveal the physical processes connecting deep and shallow deformation over different time scales (e.g., van Dinther et al., 2013b; Dal Zilio et al., 2018).

To investigate the mechanisms controlling the regional tectonics and to address the limitations of existing research, this study considers long time periods and links small-scale tectonics and seismicity to large-scale dynamics and structure using a seismo-thermo-mechanical (STM) modeling approach (van Dinther et al., 2013b). This method can simulate long-term visco-elasto-plastic deformation of the lithosphere, dislocation creep and mantle flow together with short-term brittle-plastic failure and fault slip associated with accumulated elastic stress release. This ensures that faults can for the first time be loaded tectonically by velocities and stresses resulting from slab pull. Our model setup is thus based on the hypothesis that lithospheric dynamics driven by slab pull (i.e., with no imposed shortening or extension) can largely explain the active tectonics and seismicity of the modeled retreating subduction/collision system.

We performed a series of numerical experiments to both investigate the retreating subduction/collision system and to identify a set of best-fit model parameters allowing to capture the present-day spatial distribution of compressional and extensional normal stresses and of surface velocities. This is achieved by varying the rheology of the lower crust and the temperature of the slab, the asthenospheric wedge and of the lowermost crust of Adria. Once the location of present-day tectonic regimes is broadly reproduced, the resulting seismicity and surface velocities are analyzed in comparison with observations. Subsequently, we study how these short-term features are affected by slab pull and lithospheric rheology.

2. Methodology and setup

2.1. Seismo-thermo-mechanical modeling

The STM modeling approach was developed, described, and first applied by (van Dinther et al. (2013b). This approach is based on a geodynamic numerical code that uses a fully staggered grid, conservative finite-difference scheme with marker-in-cell technique to solve for the conservation of mass, momentum and heat (Gerya and Yuen, 2007). To do so a Maxwell visco-elasto-plastic rheology is used. Drucker-Prager plasticity approximates both plastic and brittle yielding in a continuum mechanics framework and consists of plastic strain accumulation upon reaching a pressure-dependent yield strength σ_{yield}.

The constitutive relation linking deviatoric stress σ_{ij}' with strain rate $\dot{\varepsilon}_{ij}$ is thus

$$\dot{\varepsilon}_{ij}' = \underbrace{\frac{1}{2\eta}\sigma_{ij}'}_{\text{viscous}} + \underbrace{\frac{1}{2G}\frac{D\sigma_{ij}'}{Dt}}_{\text{elastic}} + \underbrace{\begin{cases} 0 & \text{for } \sigma_{II}' < \sigma_{yield} \\ \chi\dfrac{\partial\sigma_{II}'}{\partial\sigma_{ij}'} = \chi\dfrac{\sigma_{ij}'}{2\sigma_{II}'} & \text{for } \sigma_{II}' = \sigma_{yield} \end{cases}}_{\text{brittle-plastic}}, \tag{1}$$

where G is the shear modulus, $\frac{D}{Dt}$ the objective co-rotational time derivative, $\sigma_{II}' = \sqrt{\sigma'^2_{xx} + \sigma^2_{xz}}$ the second invariant of the deviatoric stress tensor, and χ a plastic multiplier which connects strain rates to stresses during yielding (Gerya and Yuen, 2007). Non-plastic effective viscosity η is computed as a function of stress according to a non-linear flow law with dependence on pressure P and temperature T:

$$\eta = \frac{\sigma_{\parallel}'^{1-n}}{2A_D}\exp\left(\frac{E_a + PV_a}{RT}\right), \tag{2}$$

with R the universal gas constant, n the exponential coefficient, A_D the pre-exponential factor, E_a and V_a the activation energy and volume (Ranalli, 1995).

Brittle-plastic yielding occurs when the stress satisfies the Drucker-Prager yield criterion, defined as

$$\sigma_{II}' = \sigma_{yield} \tag{3}$$

with yield strength

$$\sigma_{yield} = C + \mu_{eff}\,P. \tag{4}$$

Here, C is the compressive residual strength and $\mu_{eff} = \mu(1 - \lambda)$ is the effective friction coefficient, with internal friction coefficient μ and pore fluid pressure factor $\lambda = \frac{P_{fluid}}{P}$, where P_{fluid} is fluid pressure and P is total pressure. When σ_{II}' reaches the yield strength σ_{yield}, the effective viscoplastic viscosity η_{vp}, otherwise equal to η, becomes $\eta\frac{\sigma_{II}'}{\eta\chi + \sigma_{II}'}$. To allow the spontaneous nucleation, propagation and arrest of seismic events, friction depends on local slip rate V according to a strongly slip rate dependent friction formulation (e.g., Cochard and Madariaga, 1994; Ampuero and Ben-Zion, 2008), in which a relation with V in the denominator is thought to represent friction at high seismic slip rates (e.g., Di Toro et al., 2011a):

$$\mu = \mu_d + \frac{\mu_s - \mu_d}{1 + \frac{V}{V_c}}, \tag{5}$$

where static and dynamic friction coefficients μ_s and μ_d, respectively, and characteristic slip rate V_c. In our models, μ_d is set to 30% of μ_s after Di Toro et al. (2011b) and V_c is 4.4 mm yr^{-1} following van Dinther et al. (2013b). The slip rate V is computed as

$$V = 2\dot{\varepsilon}_{II,vp}\,\Delta x, \tag{6}$$

where Δx is grid size, representing the width of the fault, and $\dot{\varepsilon}_{II,vp}$ is the second invariant of the visco-plastic strain rate.

2.2. Model setup and observational constraints

The reference model setup in Fig. 2 combines a suite of geological and geophysical observations. We design the initial configuration on the basis of a geological and structural profile of Molli et al. (2010). We selected this profile because it synthesizes various geological and geophysical observations into a schematic yet detailed cross-section extending to mid-crustal depths. The faults in the profile are transposed into the model as thin zones with their own rock type. Their rheology is significantly weaker than the other rock types, and thus more prone to brittle-plastic yielding. However, yielding and seismicity can and do also occur away from prescribed faults. At depth, the profile is supplemented by published information. In particular, we adopt the Moho geometry from a cut through the model of Spada et al. (2013), based on seismic reflection and refraction as well as receiver functions. In the setup, the lithospheric mantle and thus the Moho consist of two distinct and partly overlapping segments (Adriatic and Tyrrhenian), in accordance with the receiver function study of Bianchi et al. (2010). The Adriatic lower crust in the setup follows the Moho downwards and is shaped accordingly with the low-velocity zone tomographically imaged at moderate depths (35–55 km) beneath the middle and southwestern side of the range, above the Adriatic mantle (Di Stefano et al., 2009). The lithosphere-asthenosphere boundary is located 100–120 km beneath the southern Po Plain and northernmost Apennines and around 70 km beneath the eastern coast of the Ligurian sea, in accordance with

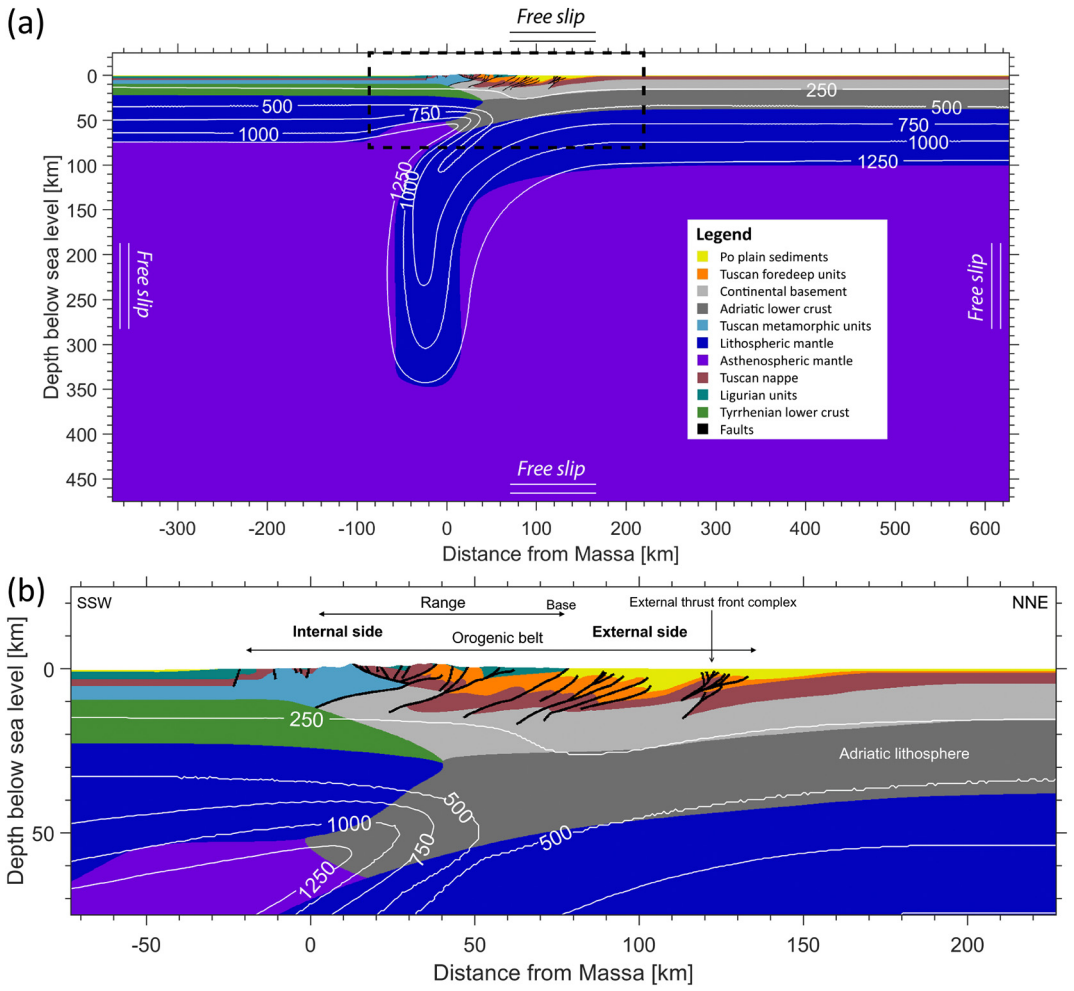

Fig. 2. Reference model setup showing the distribution of the different rock types, as well as the isotherms of the reference temperature setup (with values in °C). Topography is not vertically exaggerated. (a) Full setup with the rock type legend and the velocity boundary conditions. (b) Zoom on the area outlined in (a), showing the details of the lithospheric setup. The labels and arrows show the location of the whole orogen and of the mountain range and identify the two lithospheric domains. Horizontal distance is measured northeastwards along the profile trace starting from the city of Massa, on the coast.

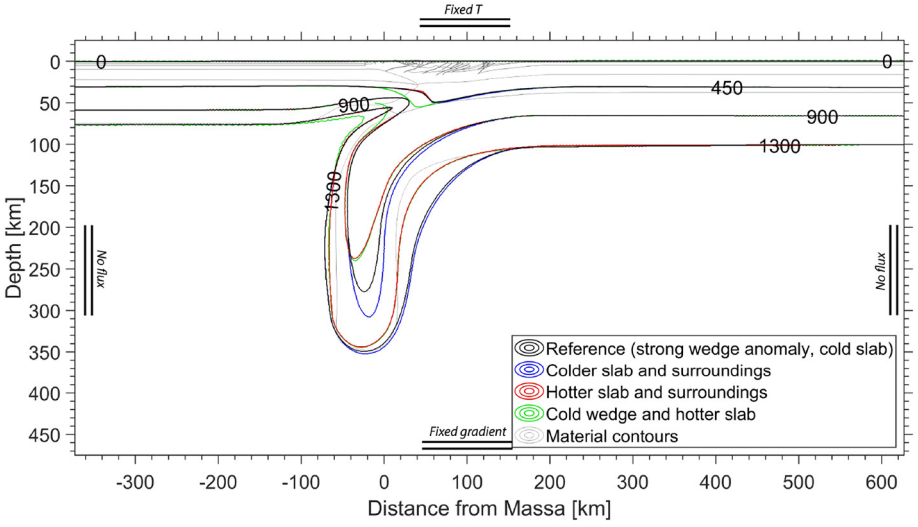

Fig. 3. Contours of different interpolated temperature setups used in the models. For each setup, the same isotherms are shown. Each color corresponds to a different temperature setup. Boundary conditions are also shown. The thin gray lines, shown as a spatial reference, are material contours.

Table 1
Rheological and other physical parameters for each material type in the reference model. For all materials, $\rho = \rho_0[1 - \alpha(T - 298)][1 + \beta(P - 0.1)]$ and $\mu_d = 0.3\mu_s$. All rock types (faults included) have $\alpha = 3 \cdot 10^{-5}\ ^\circ\mathrm{C}^{-1}$, $\beta = 10^{-5}\ \mathrm{MPa}^{-1}$, and $C_p = 1000\ \mathrm{J kg}^{-1}\ ^\circ\mathrm{C}^{-1}$. Air has $\alpha = 0\ ^\circ\mathrm{C}^{-1}$, $\beta = 0\mathrm{MPa}^{-1}$, and $C_p = 3.33 \cdot 10^6\mathrm{J kg}^{-1}\ ^\circ\mathrm{C}^{-1}$. μ_s is 0.3 on faults, 0.8 in the mantle, 0.6 in other rock types and 0 in air. λ is 0.4 in the mantle and lower crusts, 0.6 elsewhere. The physical quantities corresponding to each symbol and the sources for the values used are specified in Table 2.

Symbol	$1/A_D$	n	E_a	V_a	G	C	μ_s	λ	ρ_0	k	H_r
Units	$\mathrm{Pa}^n \cdot \mathrm{s}$	–	kJ	$\frac{\mathrm{J}}{\mathrm{bar}}$	GPa	MPa	–	–	$\frac{\mathrm{kg}}{\mathrm{m}^3}$	$\frac{\mathrm{W}}{^\circ\mathrm{C\,m}}$	$\frac{\mathrm{nW}}{\mathrm{m}^3}$
Sticky air	$1.00 \cdot 10^{17}$	1.0	0.00	0.0	700	0	0	0	1	200	0
Po Plain sediments	$1.97 \cdot 10^{17}$	2.3	154	0.6	50	3	0.6	0.6	2800	$\left[0.64 + \frac{807}{T+77}\right]e^{4\cdot10^{-6}P}$	1500
Tuscan foredeep units	$1.97 \cdot 10^{17}$	2.3	154	0.8	50	5	0.6	0.6	2800	$\left[0.64 + \frac{807}{T+77}\right]e^{4\cdot10^{-6}P}$	1500
Continental basement	$1.97 \cdot 10^{17}$	2.3	154	1.2	50	10	0.6	0.6	2900	$\left[0.64 + \frac{807}{T+77}\right]e^{4\cdot10^{-6}P}$	1000
Adriatic lower crust											
Mafic granulite	$1.13 \cdot 10^{21}$	4.2	445	0	120	5	0.6	0.4	2900	$\left[1.18 + \frac{474}{T+77}\right]e^{4\cdot10^{-6}P}$	250
Plagioclase (An75)	$4.80 \cdot 10^{22}$	3.2	238	0	25	5	0.6	0.4	3000	$\left[1.18 + \frac{474}{T+77}\right]e^{4\cdot10^{-6}P}$	250
Wet quartzite	$1.97 \cdot 10^{17}$	2.3	154	0	10	5	0.6	0.4	3000	$\left[1.18 + \frac{474}{T+77}\right]e^{4\cdot10^{-6}P}$	250
Tuscan metamorphics	$2.80 \cdot 10^{22}$	3.2	238	0.8	50	26	0.6	0.6	2900	$\left[1.18 + \frac{474}{T+77}\right]e^{4\cdot10^{-6}P}$	250
Mantle (lithosphere)	$3.98 \cdot 10^{16}$	3.5	532	0.8	50	5	0.8	0.4	3300	$\left[0.73 + \frac{1293}{T+77}\right]e^{4\cdot10^{-6}P}$	22
Mantle (asthenosphere)	$3.98 \cdot 10^{16}$	3.5	532	0.8	50	5	0.8	0.4	3300	$\left[0.73 + \frac{1293}{T+77}\right]e^{4\cdot10^{-6}P}$	22
Tuscan nappe	$1.97 \cdot 10^{17}$	2.3	154	1.2	50	19	0.6	0.6	2850	$\left[0.64 + \frac{807}{T+77}\right]e^{4\cdot10^{-6}P}$	1000
Ligurian units	$1.97 \cdot 10^{17}$	2.3	154	1.2	50	4	0.6	0.6	2800	$\left[0.64 + \frac{807}{T+77}\right]e^{4\cdot10^{-6}P}$	1000
Tyrrhenian lower crust	$1.25 \cdot 10^{21}$	4.2	154	0.8	50	5	0.6	0.4	2800	$\left[1.18 + \frac{474}{T+77}\right]e^{4\cdot10^{-6}P}$	250
Faults	$5.01 \cdot 10^{25}$	4.0	154	0.8	12	1	0.3	0.6	2900	$\left[1.73 + \frac{1293}{T+77}\right]e^{4\cdot10^{-6}P}$	22

Table 2
Symbols and sources of physical parameters used in the models.

Quantity	Symbol
Inverse of pre-exponential factor[a]	$1/A_D$
Flow law exponent[a]	n
Activation energy[a]	E_a
Activation volume[a]	V_a
Shear modulus	G
Compressive residual strength	C
Static shear modulus[c]	μ_s
Pore-fluid pressure factor	λ
Reference density	ρ_0
Thermal conductivity[b,d]	k
Radiogenic heat production	H_r

[a] From Ranalli (1995).
[b] From the corresponding generic rock types from Clauser and Huenges (1995).
[c] Chosen on the basis of the values for generic rock types used in previous STM work (van Dinther et al., 2013a, and references therein] and of the mixes of lithologies present in the orogen (Molli, 2008; Cerrina Feroni et al., 2002).
[d] In the formulas, P and T are in SI units.

the surface wave tomography of (Panza et al. (2003). We add a sub-vertical slab of lithospheric Adriatic mantle down to depths of 400 km, following the teleseismic tomography of Benoit et al. (2011). The uncertainty in the depth extent of the lithospheric mantle is implicitly addressed in the different temperature setups used (Fig. 3 and Section 3.3), since it is temperature that distinguishes the lithospheric and asthenospheric mantle in terms of rheology and density (Tables 1 and 2).

The reference set of material properties corresponding to each rock type is shown in Table 1. Three different lower crustal rheologies are tested, as their ductility is expected to control the style of deformation. Following Faccenda et al. (2009) and Ranalli (1995), these are mafic granulite, plagioclase, and wet quartzite.

The model temperature field is initialized on the basis of a self-consistent simulation of retreating subduction with a generic initial geometry. The initial temperature field accounts for model geometry and includes a cold accretionary crustal wedge, a hot asthenospheric wedge, and a lithosphere-asthenosphere boundary at around 1300 °C. The maximum depths of earthquake hypocenters between 2005 and 2015 (Chiarabba and De Gori, 2016) are used as a broad indicator of the location of the thermally determined brittle-plastic transition, keeping in mind that seismicity has been observed beneath the Apennines in hotter areas than normally expected (Pasquale et al., 2010). The isotherms in the asthenospheric mantle follow an adiabatic thermal gradient of ~0.5 °C km^{-1} (Katsura et al., 2010). The top of the crustal basement has a temperature of around 200 °C, in accordance with the thermal model inverted by (Pasquale et al. (2013). For the initial thermal setup, temperature contours are designed with 100 °C) intervals. These contours are then interpolated to the entire temperature field using a biharmonic splines method. The location of any specific isotherm is uncertain to a large degree. To explore such uncertainty and consider at least partly the possible range of temperatures, we also test alternative versions of the temperature field. In particular, we vary the isotherms in the poorly constrained areas that might control the large-scale tectonic regime: (i) the subducted slab and (ii) the deep suture area between Adriatic and Tyrrhenian lithospheres (Fig. 3).

2.3. Model specifications

The boundary conditions used are free-slip on all boundaries and zero lateral P gradient at the four corners (with $P = 0$ at the top). Lateral boundaries are zero-heat-flux, while the top has fixed T (0 °C) and a fixed T gradient (2.413 °C km^{-1}) at the bottom. A 25-km-thick weak "sticky air" layer ($\sigma_{yield} = 0$, $\rho = 1\ \mathrm{kg\ m}^{-3}$, $\eta = 10^{17}$ Pa s) was placed at the top to approximate a free surface (Crameri et al., 2012). The models have a variable spatial resolution, from 250 m in the area of interest to 5 km at the edges and bottom. To minimize boundary effects,

the model space extends vertically for 500 km and horizontally for 1000 km.

2.4. Modeling procedure

Following Dal Zilio et al. (2018), we run the models in two phases: (i) long-term, with timestep $\Delta t = 200$ yr, and (ii) short-term, with $\Delta t = 1$ yr. The long-term phase allows the model to develop self-consistent stresses and velocities and attain isostatic equilibrium. Once the stress configuration and crustal velocities are broadly consistent with present-day observations, the timestep size is progressively reduced to 1 yr. We then switch to the short-term phase, during which the model is run for 20,000 years and spontaneous events are simulated.

2.5. Evaluation of model seismicity

Due to computational challenges, we use a constant timestep of 1 yr during the short term modeling phase. Hence, seismic slip rates cannot be achieved. For the purpose of this paper, we focus on the type, distribution and size of events and do not attempt to realistically simulate the rupture process. To detect events, we record all occurrences of relative displacement (slip) along localized, spontaneous plastic shear bands that experience a substantial increase in slip rate and permanent stress drop, following Dal Zilio et al. (2018). We use a stress drop threshold of 0.5 MPa (Allmann and Shearer, 2009) and a slip rate threshold of 4×10^{-9} ms^{-1}. The detection algorithm groups into the same event all model markers that are are undergoing brittle-plastic yielding, meet the thresholds, and are within a timestep and grid step of each other. To relate events size to the most common quantity describing earthquake size, we compute the total (3D) moment magnitude M_w from width W (in km) using the empirical scaling law

$$M_w = a + b \log_{10}(W), \tag{7}$$

with the empirical coefficients $a = 3.8049$ and $b = 2.4390$ calculated by Blaser et al. (2010) via orthogonal least-squares regression. We only consider events with $M_W \geq 3.5$, corresponding to 3 grid steps in the densest part of the model. The markers within each event that yield at the earliest time define the hypocentral region.

3. Results and analysis

3.1. Lithospheric and crustal dynamics

The present-day distribution of velocities and stresses in the study area of the northern Apennines can be broadly reproduced by our reference model through the combination of high temperatures in the mantle wedge and lowermost crust and the most ductile (wet quartzite) lower crust rheology (Figs. 3 and 4). These parameters allow mantle material to protrude upward and northward at relatively high velocity (~20 mm yr^{-1}) into the lower crust. As a result, a hot, low-viscosity, increasingly weak channel forms above the Adriatic lithospheric mantle. This decouples the overlying upper crust, which includes the mountain range, from the slab and pushes upward and laterally with respect to the Tyrrhenian domain further to the southwest, causing uplift and extension. Conversely, the portion of the upper crust ahead of the low-viscosity channel, including the Po Plain, is compressed by the protruding material. It is also still mechanically coupled to the partly delaminated, sinking lithospheric mantle slab and therefore subsides. Two tectonic regimes thus form in the upper crust: extension and uplift throughout the range versus compression and subsidence in the foreland (Fig. 4). This is in agreement with present-day observations.

In contrast, the use of the strongest (mafic granulite) lower crust rheology, produces a rheological coupling of the slab to the upper crust, regardless of temperatures. This leads to tectonic regimes opposite to the observed in the study area, with thrusting and subsidence in the range and extension and uplift in the Po plain (Fig. 5).

On the other hand, the intermediate (plagioclase) rheology of the lower crust allows for wedge protrusion and lithospheric delamination only when the lower crust is brought to temperatures of over 450 °C. However, normal stresses in the range are partially compressional, the deep area 20–35 km underneath the base of the mountain range is not entirely compressional, and the foreland beyond the external thrust front undergoes intense extension and uplift (Fig. 5).

With further modeling, we attempt to produce realistic tectonic regimes with less ductile lower crust, such as by imposing a zone of eclogitic material or a localized shear zone at the deep suture between the two lithospheric domains. These efforts did not lead to compression throughout the Po plain without significant changes in the defined initial crustal and lithospheric geometry. Therefore, the simulations suggest that the simultaneous presence of the two tectonic regimes observed at present day requires high temperatures in the mantle wedge and lowermost crust.

3.2. Seismicity and surface deformation

We analyze the short-term behavior of the reference model in terms of surface displacement and seismicity.

3.2.1. Surface velocities

Horizontal model velocities show less than 2 mm yr^{-1} of extension distributed throughout the external half of the mountain range and ~ 3 mm yr^{-1} of convergence across the whole of the Po plain. A similar trend is present in GPS measurements by Devoti et al. (2011) with respect to stable Eurasia (Fig. 6). In general, we found model velocities 1.5 − 2 mm yr^{-1} lower than observed, probably due to the northeastward drift of the northern Adriatic domain (Mantovani et al., 2015b), which we do not model. Horizontal velocities in the plain and in the most external and internal parts of the range are in good agreement with most of the GPS velocity data from Bennett et al. (2012). Model velocities describe horizontal shortening between the base of the range and the external buried thrust front as well as extension in the middle and external side of the chain. Vertical model velocities in the Apennines are compatible with some GPS observations, especially those by Bennett et al. (2012). In general, however, GPS data do not show consistent uplift in the mountain range like the models do. Furthermore, in the foreland the modeled subsidence peak is relatively low in amplitude (less than 5 mm yr^{-1}) and extends across the whole plain.

3.2.2. Seismicity and stresses

Crustal stresses in the reference model are extensional underneath the Apennines and compressional throughout the Po Plain (Fig. 4). Average deviatoric shear stresses σ_{xy}' reach their highest magnitudes in the middle of the Po plain, in the external thrust front. Most of the modeled seismic moment release occurs in this area, both on the prescribed faults and in off-fault events. Modeled earthquakes also occur on thrusts around the base of the range, which produce fewer earthquakes than the external thrust front itself (Fig. 4). This is in agreement with both instrumentally observed and historical seismicity, which tend to cluster on the external thrust front complex. Extensional crustal seismicity in the reference model is focused in the middle of the mountain range and is absent in its most internal part (distance along the profile $x < 25$ km). This is in agreement with earthquake locations observed tens of kilometers to the southeast and with the proposed source of the $M_w \approx 6.5$ Lunigiana-Garfagnana earthquake of 1920 (Rovida et al., 2016). Nevertheless, several earthquakes have been observed instrumentally along our reference profile at $x < 25$ km (Chiarabba et al., 2005). The largest events in the model have a M_W of 7.4.

Reference model seismicity also includes events in the lithospheric mantle, at the top of the Adriatic slab. These occur on spontaneously formed normal faults located in the external hinge area of the bending

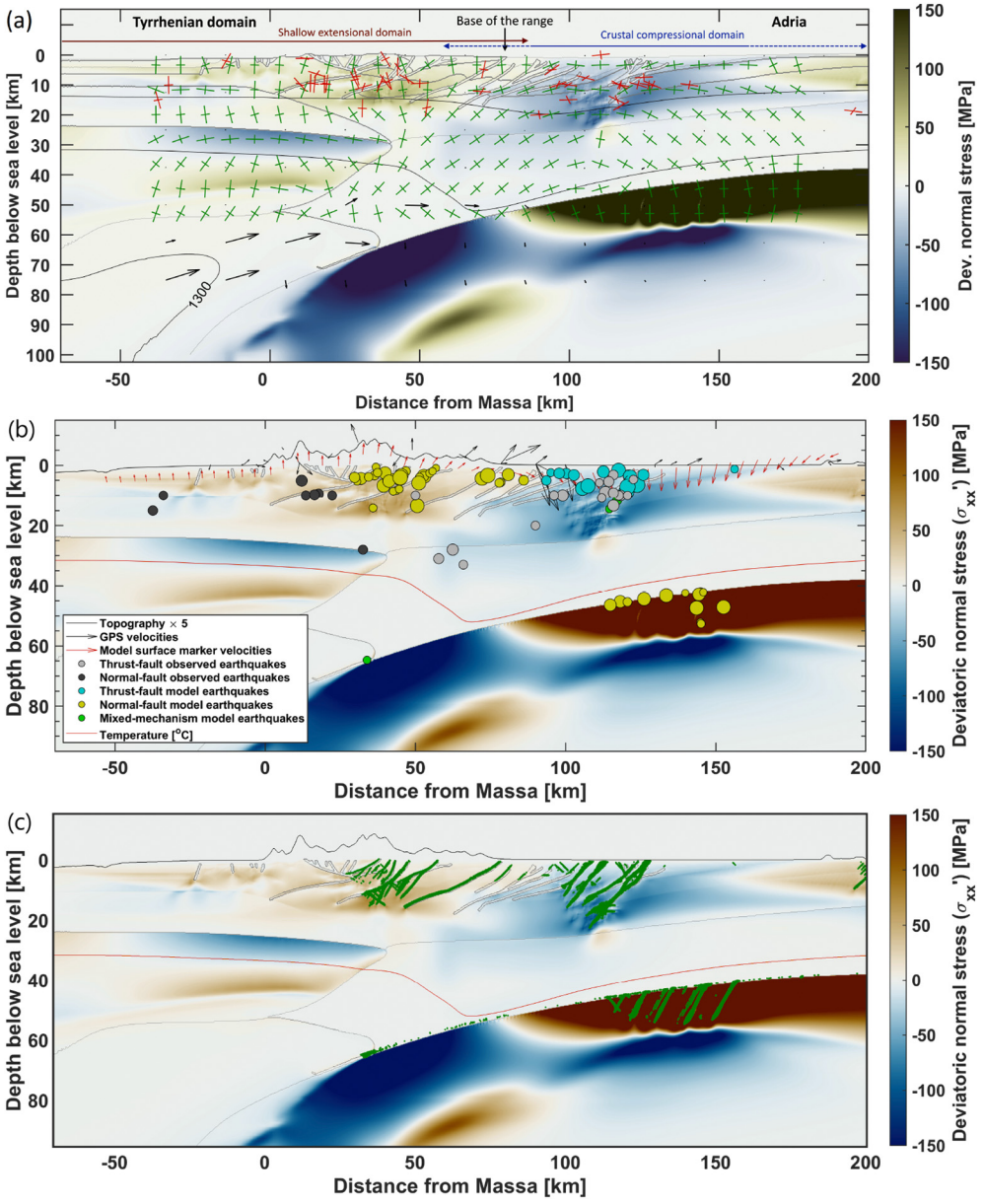

Fig. 4. Deformation features of the reference model in comparison with observations. Deviatoric normal stresses are shown in the background. All stresses are taken from the last timestep of the model. (a) Principal stress axes and velocity vectors in the reference model. (b) Event hypocenters and surface velocities at the end of the short-term model phase. (c) Locations of all markers involved in events. Observed stress axes, velocities, and hypocenters are projected onto the profile from within 40 km of horizontal distance. The compressional (long) and extensional (short) principal stress axes are shown in brown for the model and in cyan for World Stress Map observations (Heidbach et al., 2016). In (a), velocities are in 50,000:1 scale with respect to the plot axes: a length of 1 in the reference frame of the axes corresponds to 20 mm yr $^{-1}$. In (b) and (c), the topography is vertically exaggerated. In (b), velocity arrows represent the average yearly displacement in 500,000:1 scale. The faulting style of model earthquakes is determined by the average coseismic orientation of principal strain rate axes (extension closer to the horizontal than vertical direction for normal faulting, vice versa for thrust faulting) and average horizontal normal stress (positive for normal faulting, negative for thrust faulting) of the markers in each event. Observed earthquake hypocenters are selected from an updated version of the CMT catalog of Pondrelli et al. (2006) and plotted as circles with diameter proportional to M_w. Only events with $M_w \geq 3.5$ are considered in both observed and model seismicity. (For interpretation of the references to color in this figure legend, the reader is referred to the web version of this article.)

slab (Fig. 4). Overall, the depth distribution of model earthquake hypocenters is bimodal, with a peak in the upper crust and one in the bending slab, and no events in the lower crust (Fig. 7). However, the cluster of instrumentally recorded earthquakes underneath the external thrust front only shows focal locations at middle- to -lower crustal depths (25–45 km), rather than in the lithospheric mantle

3.3. Slab pull controlling the distribution of seismicity

In a novel development, we directly link slab pull and events in the same simulation. To explore the importance of slab pull in driving the dynamics of the northern Apennines, we perform two numerical experiments. In these experiments, we use alternative temperature setups (Section 2.2 and Fig. 3) with different isotherms in and around the slab, thus altering its buoyancy. This also allows us to explore the effect of different mantle temperatures on model dynamics, which is important given the lack of knowledge of the deep thermal conditions. Higher slab temperatures, corresponding to a lower average density and less negative buoyancy and thus to less slab pull, decrease the intensity of crustal deformation (Fig. 8). Conversely, lower temperatures increase slab pull and the intensity of deformation. This occurs despite the absence of strong mechanical coupling between the upper crust and the slab (Fig. 3). The effect of slab temperatures on deformation is manifested in the total seismic moment released and in seismic rates (Fig. 8). In fact, the hotter slab reduces the moment released in both crustal regimes to around 20% of its value in the reference model (17% in the extensional crustal domain, 21% in the compressive one). The seismic rate in the crust is also reduced, though more unevenly in the two regimes. The seismic rate in the mountain range under extensional stresses is reduced by 68% and becomes 60% of that in the active thrust belt, where the reduction is by 50%. The different magnitude of the effect of slab temperatures on seismic moment release and on seismic rates is consistent with the distribution of model stresses and seismicity. In particular, in the reference model the compressional regime has a lower proportion of smaller earthquakes than the extensional one, as well as larger $|\sigma_{xx}'|$ and σ_{II}'. This is consistent with the inverse relationship between the Gutenberg-Richter b value and differential stress $\Delta\sigma$ observed in the laboratory (Amitrano, 2003), in earthquakes in continental areas (Scholz, 2015), and in STM modeling of orogenic belts (Dal Zilio et al., 2018). Therefore, the seismic rate in the extensional

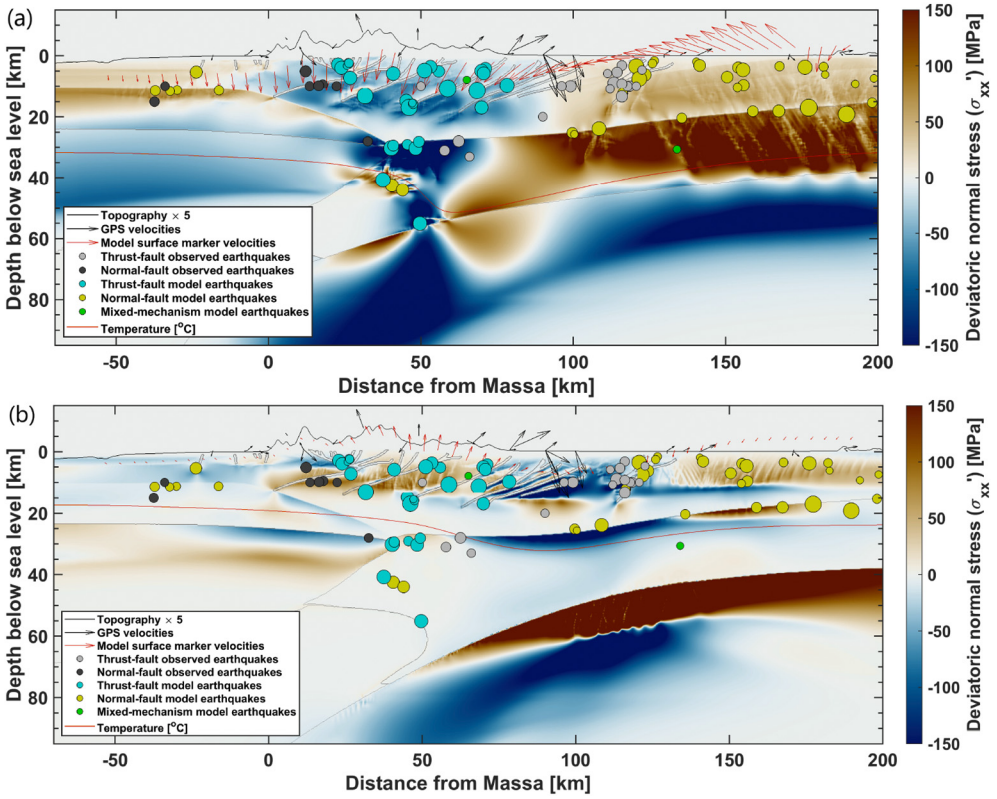

Fig. 5. Comparison with observations of the deformation features of different models. (a): mafic granulite lower crusts and the same temperature setup as the reference model (hot mantle wedge, cold slab). The resulting pattern of tectonic regimes is opposite as what is observed in the Northern Apennines, with thrust-related seismicity and subsidence in the mountain range and with seismogenic extension and uplift in the plain. (b): plagioclase lower crusts and a hot lithosphere and slab. Lithospheric delamination-retreat and wedge protrusion are occurring. However, the mountain range is partly compressional and the external Po plain intensely extensional and uplifting, and the Moho geometry has deformed significantly from the initial setup. Observed topography, observed and model velocity arrows and earthquake hypocenters by faulting mechanism, and model stresses and material contours are shown as in Fig. 4.

regime is more susceptible to weaker driving forces, as even a small reduction in crustal stresses stops the small extensional earthquakes from occurring. The influence of slab temperatures on crustal deformation is also evident in the surface velocities: the colder, more buoyant slab increases horizontal and vertical velocities, while the hotter slab has the opposite effect (Fig. S1). Based on our results, we can conclude that the lateral distribution of relative earthquake frequency and seismic moment release in the studied migrating orogen is critically controlled by the slab pull driving this system.

3.4. Effect of lithospheric mantle stiffness on seismicity

The impact of elastic properties of the lithospheric mantle on shallow tectonics is typically thought to be negligible. We evaluate this impact by varying its elastic stiffness. A higher shear modulus G in the lithospheric mantle leads to a stiffer, more rigid slab, which generally reduces slab bending and lithospheric delamination. As a consequence, less crustal deformation occurs. Therefore, generally less seismic moment is released in the crust, especially in the compressional domain (Fig. 9). The vertical components of model surface velocities are also affected (Fig. S2). In particular, they decrease by up to ~ 1 mm yr^{-1} in the external part of the mountain range (thus reducing uplift) and in the plain (which amounts to faster subsidence). Despite a general negative trend, the change in released seismic moment and vertical surface velocities with increasing slab G is variable. This could be due to a trade-off between two processes: on one hand, the lithospheric mantle undergoes less bending in response to the unchanged dynamic load. This forces the deformation due to hot mantle wedge and lower crust protrusion to localize to a greater extent in the crust, rather than in the bending and downwelling of lithospheric mantle. On the other hand, greater stiffness slows down slab bending and thus overall deformation through reducing crustal loading rates. Such influence of slab stiffness on seismicity demonstrates the importance of complex interactions between different subsurface regions. Furthermore, it shows that small changes in stresses and displacements due to preperties of material at sub-crustal depths (greater than 40 km) contribute to determine the lateral distribution and abundance of earthquakes.

3.5. Effect of rock strength on earthquake distribution

We also investigate the influence of the yield strength parameters on short-term tectonics in the models. Yield strength is expected to strongly affect local stresses and the specific distribution of seismicity, while having a negligible effect on the overall stress and velocity pattern. The results of such experiments are presented and discussed in Appendices A and B. We find that both bulk rock strength and fault friction (which determines fault strength) do influence the intensity and distribution of simulated seismicity. In particular, higher or lower bulk strengths accordingly increase or decrease the seismic moment M_0 released. The effect on total seismic rate in the different regimes is not uniform, because the distribution of the released seismic moment over different magnitudes is not constant and depends on the specific combination of model parameters. Fault friction, instead, affects seismic M_0 release in a less consistent way. Both decreasing and increasing fault friction reduce the M_0 released in the extensional regime. Conversely, the effect of increasing friction on M_0 release in the compressional regime is monotonic. This implies that the lateral distribution of the intensity of seismicity, in terms of M_0 release, is significantly affected by fault friction, because of the different stress loading regimes active in different areas of the model.

Overall, the strength of bulk rock and of predefined faults determine the specific lateral distribution of seismicity across the model. However, the magnitude of the impact of strength, especially of bulk rock, on seismic moment release is not dominant with respect to the effect of the temperature and stiffness of the lithospheric mantle (Sections 3.3 and 3.4). Therefore, our simulations suggest that the elastic and thermal properties of deep material, in the particular geodynamic setting of the northern Apennines, can be of comparable importance in controlling crustal seismicity as the mechanical strength of the crust. This is a significant result, given that rock and fault strength are usually paid

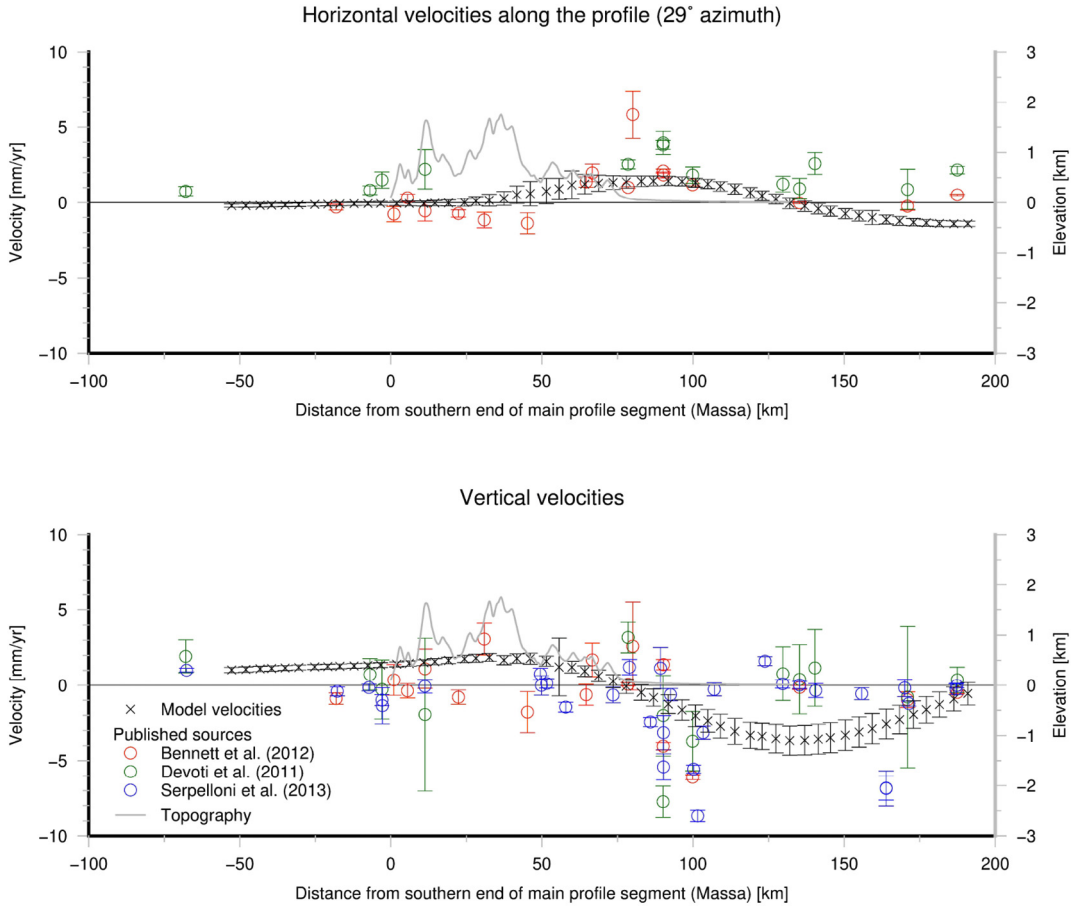

Fig. 6. Average horizontal and vertical velocities of markers placed at the surface of the reference model. Vertical velocities are positive upwards. Only interseismic time periods between major events are considered. Published GPS velocities are shown for comparison, projected from within 40 km of the profile. Note that velocities from Bennett et al. (2012) are relative to the centroid of the regional GPS network used, whereas Devoti et al. (2011) take stable Eurasia as the reference frame and Serpelloni et al. (2013) use a global reference frame (ITRF2008). The Vertical bars correspond to an uncertainty of one standard deviation (1σ). Topography is outlined in light gray for orientation purposes.

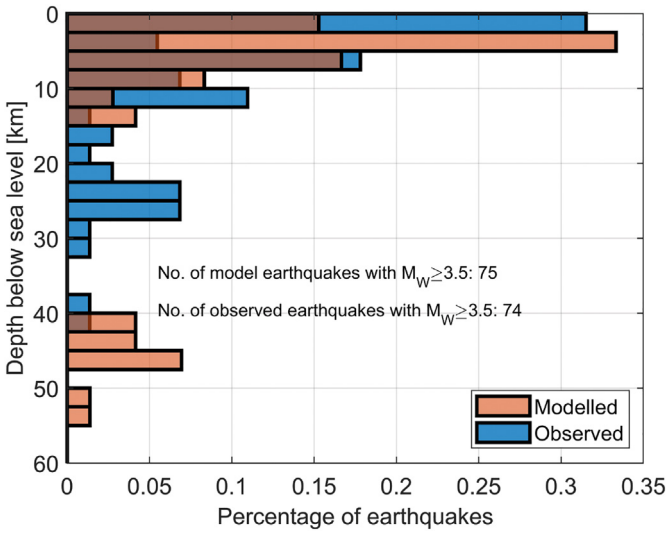

Fig. 7. Depth distribution of earthquakes in the reference model. The relative depth distribution is compared with that of events in the updated instrumental seismicity catalog of Chiarabba et al. (2005) within 25 km of horizontal distance from the profile.

much more attention than any deep properties when studying seismicity on complex fault systems.

4. Discussion

4.1. Deformation

4.1.1. Surface deformation and GPS observations

The horizontal components of model velocities delineate moderate surface extension in the external part of the range and shortening in the adjacent Po plain foreland, in agreement with GPS observations by Devoti et al. (2011). Vertical model velocities delineate the pattern of uplift in the mountain range and subsidence in the foreland generally observed for the Northern Apennines. Upward model velocities are in agreement with exhumation rates estimated near the southwestern end of our reference profile (~0.7 mm yr^{-1} on average, 1.8 mm yr^{-1} maximum; Balestrieri et al. (2003)). However, present-day vertical velocities from GPS observations show a roughly even mix of uplift and subsidence in the mountain range (Fig. 6). This suggest that either localized deformation overprints the slow uplift signal, or that broad tectonic uplift has recently ceased.

The downward velocities produced in the models form a broad peak more than 100 km wide. Conversely, in GPS observations directly along the profile, subsidence in the Po plain is focused in the vicinity of the range and reaches rates of 8 mm yr^{-1} or more. However, results from the geodetic study of Serpelloni et al. (2013) are in better agreement with the subsidence rates produced in the model. In particular, their

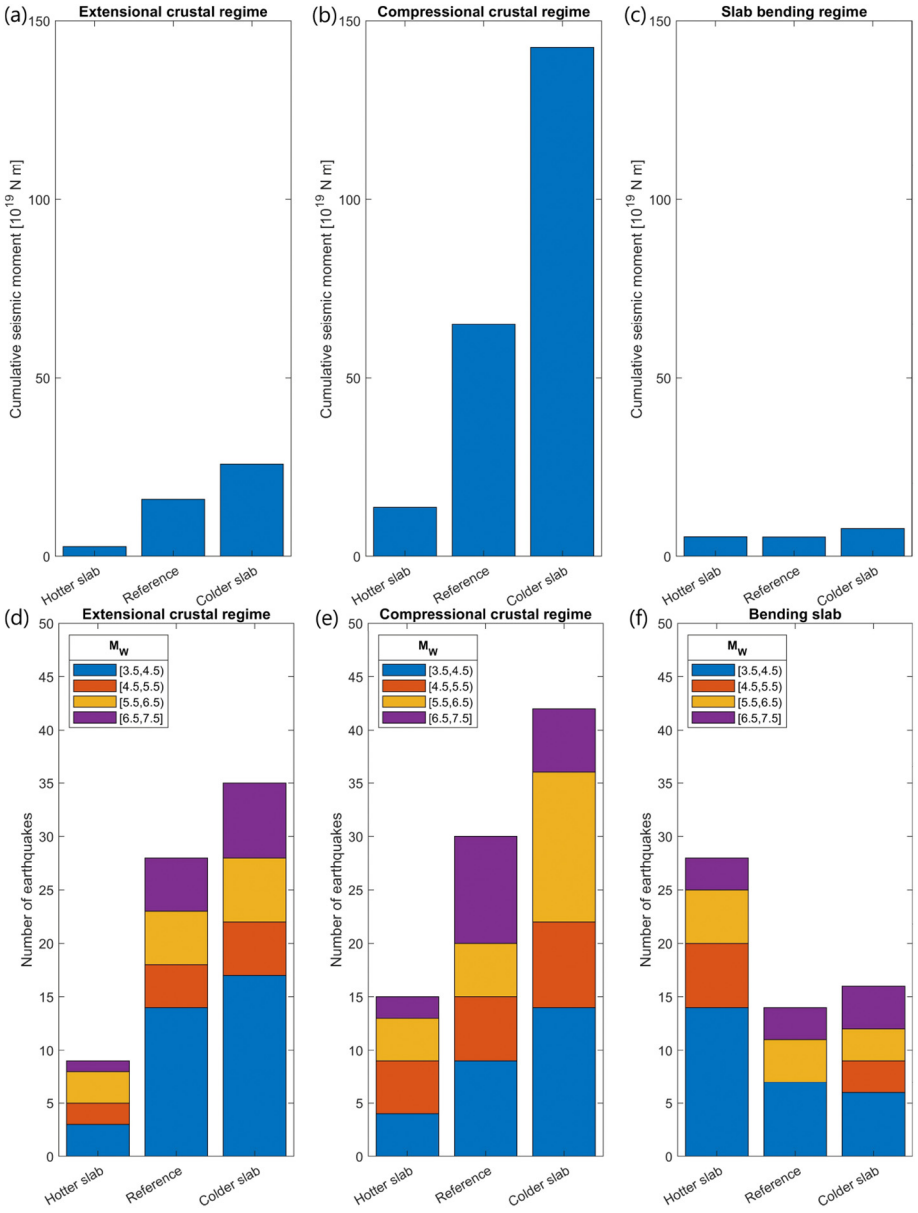

Fig. 8. Comparison of the total released seismic moment M_0 (a–c), and number of earthquakes (d–f) in models with different temperatures in and around the slab. The isotherms corresponding to the different temperature setups used are shown in Fig. 3. Increasing slab pull increases the seismic moment released in both the extensional and compressional regimes of the upper crust. It also increases the seismic rate in the crust and lowers it in the mantle. The two crustal regimes and the lithospheric mantle slab are selected manually. Only earthquakes with $M_w \geq 3.5$ are considered.

best-fit smoothed spline along a line ~50 km to the southeast of our profile defines an 80-km-wide peak beginning with an amplitude of less than 4 mm yr^{-1}. This suggests that subsidence in the eastern part of the Po Plain might be compatible with a lithospheric-scale velocity field dominated by lithospheric delamination and slab flexure and retreat, as proposed by Carminati et al. (2003). The lack of a lithospheric delamination-retreat signal in the vertical velocities observed along our reference profile could result from slab retreat and flexure being significantly slower or currently absent altogether to the northwest of the lithospheric tear proposed by Piccinini et al. (2014). Alternatively, shallow crustal processes such as fault creep and sediment deposition might mask the signal of lithospheric delamination-retreat.

4.1.2. Geodynamics

Our results show that the characteristic tectonic configuration of the Northern Apennines can be explained by lithospheric and asthenospheric dynamics driven only by the buoyancy anomalies of the slab and mantle wedge through partial decoupling and retreat of the downgoing lithosphere, in agreement with inferences of previous studies (e.g., Ventura et al., 2007; Picotti and Pazzaglia, 2008). In particular, slab buoyancy and viscous flow in the hot lower crust and mantle wedge drive lithospheric delamination and slab retreat and reproduce the tectonic regimes of the orogen (Fig. 4). This geodynamic configuration fits well within the larger framework of the entire Western Mediterranean back-arc system being driven by upper mantle–scale convection cells associated with slab retreat, back-arc extension and dynamic topography (Faccenna et al., 2014a). In this context, our modeling results clarify how viscous flow and resulting dynamic topography relate to the observed tectonics and pattern of uplift and subsidence. We find that dynamic subsidence coupled with horizontal shortening affects the external part of the orogen and the Po plain, where the upper crust is coupled with the lithospheric slab. The internal, southwestern part of the orogen undergoes active uplift and extension as a consequence of upward and outward flow of hot material

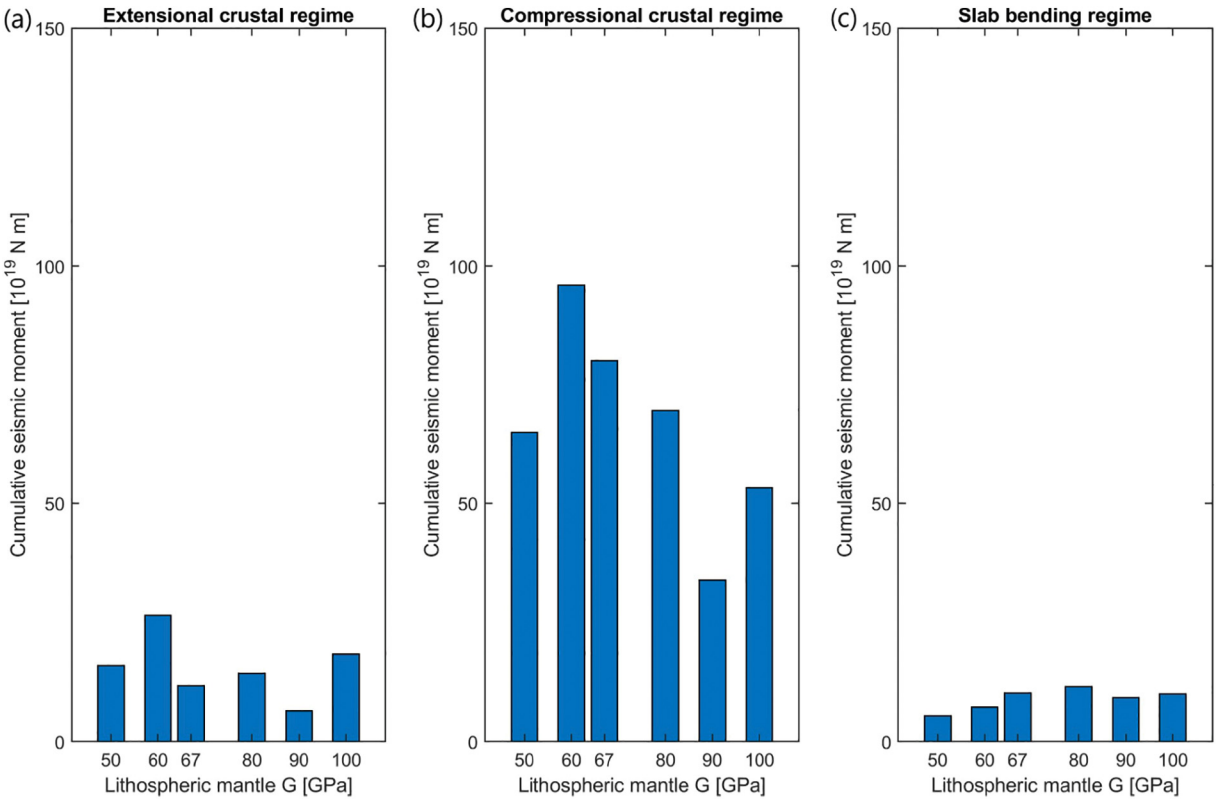

Fig. 9. Comparison of the total seismic moment M_0 in models with different shear modulus G in the lithospheric mantle. Slab stiffness affects the lateral distribution of crustal seismicity. The two crustal regimes in (a) and (b) and the bending lithospheric mantle hinge regime in (c) are considered separately and selected manually, looking at the distribution of events in space. Only earthquakes with $M_w \geq 3.5$ are considered.

in the upper mantle and lower crustal wedge. We successfully reproduce the coupling of modest uplift with horizontal extension and subsidence with compression that characterizes the Northern Apennines. The two tectonic regimes of our models are coupled and migrate gradually towards the foreland as a result of continued lower crustal wedge protrusion and lithospheric delamination-retreat, consistently with the observed northeastward migration of both the external thrust front and of the locus of extension over the past 30 Ma (Jolivet and Faccenna, 2000; Faccenna et al., 2001).

Producing lithospheric delamination associated with slab retreat in our models requires the presence of ductile and buoyant material near the contact between the Adriatic and Tyrrhenian-Ligurian domains. Such material properties are obtained in the models through a wet quartzite rheology for the Adriatic lower crust together with high temperatures. The importance of ductile lower crustal material decoupling the upper crust and lithospheric mantle, shown by our models (Figs. 4 and 5), is consistent with previous studies. In particular, Benoit et al. (2011) explain the deep structure and magmatism of the Northern Apennines in terms of lithospheric mantle delamination, which requires a rheological weakness of the lower to middle crust. Furthermore, the rheology of Adriatic middle-lower lithosphere was inferred to control the tectonic style of the orogen by Chiarabba et al. (2014). They proposed a mechanism of propagation of the tip of the asthenospheric wedge that resembles the protrusion of asthenospheric and lower crustal material in our simulations, although they do not attempt to simulate such mechanism or its enabling conditions and tectonic effects.

Our approach imposes inferred present-day structure on the model setup and therefore cannot properly simulate the long-term geodynamic evolution that led to the current configuration of the orogen. Nevertheless, the agreement of our results with the obsberved and inferred features of the orogen indicates that the geodynamic regime in our model captures the fundamental processes that shape the Northern Apennines. In particular, the deduced presence of ductile lower crustal flow, agreement between model uplift rates and geological evidence of exhumation rates (Section 4.1.1), and presence of the two characteristic and opposing tectonic regimes with corresponding types of seismicity suggests that the model captures the geodynamic processes of lithospheric delamination-retreat and back-arc uplift and extension that have built the Northern Apennines and shaped other orogens in the Mediterranean region. Therefore, although our models specifically simulate the Northern Apennines, our results could also be relevant for other locations where similar processes and features occur. This particularly holds where previous studies inferred the presence of highly ductile or molten lower crust associated with slab rollback, trench retreat and back-arc extension, such as in the Aegean (e.g., Jolivet and Brun, 2010; Jolivet et al., 2013; Ersoy and Palmer, 2013; Menant et al., 2016; Kruckenberg et al., 2011).

The ductile lower crust and resulting asthenospheric wedge protrusion in the models could not reproduce the thrust-related seismicity observed beneath the external part of the mountain range, at horizontal distances along the profile around 60 km and at mid-crustal depths (Fig. 4). This supports the idea that ductile deformation beneath the Tyrrhenian Moho is not dominant in the western sector of the Northern Apennines, while crustal underplating is likely taking place. Such an interpretation of regional tectonics was proposed by Thomson et al. (2010) from thermochronological observations. It is also supported by Chiarabba et al. (2014), who in fact restrict their hypothesized mantle nose mechanism to the more southeastern part of the orogen. Nevertheless, the models indicate that ductility of deep material at the Tyrrhenian-Adriatic suture and ongoing lithospheric mantle retreat are needed to obtain realistic stress distribution pattern. This is the case, at least, given the assumptions of buoyancy-driven dynamics and predominantly axis-parallel deformation that underlie our model setup.

4.2. Seismicity

Earthquake magnitudes seem realistic, though the maximum values (up to M_W 7.4) are significantly larger than those of any known historical event (M_W 6.5 maximum). In the reference model, 19 events larger than any observed earthquake (M_w in the 6.5–7.5 interval) occur in the 20,000 years simulated. If these simulations indeed reflect the true possible maximum event size, events larger than those known from the historical record of the last five centuries are long overdue and may occur in the near future. Alternatively, the models may overestimate the maximum possible event size in the area or its frequency of occurrence. For instance, a single event in the model might correspond in reality to multiple episodes of aseismic and seismic slip, or the rheology of crustal layers might be overly prone to yielding.

Extensional seismicity in the models occurs on major faults—including reactivated thrusts—underneath the crest of the range, while compressional crustal seismicity is focused on the external thrust front complex. This is in agreement with the observed hypocenter locations and focal mechanisms in an update version of the catalog of Pondrelli et al. (2006).

The moderately deep seismicity (deeper than 20 km) observed underneath both the base of the range and the external thrust front is not reproduced in the models (Figs. 4 and 7). This suggests that the models might not be fully capable to capture the rheological structure of the orogen. In particular, a higher-viscosity and more brittle lower crust in the Adriatic foreland may be present. However, such brittle lower crustal material, if present, is likely to be localized to a relatively small area, since highly ductile material is needed at mid-crustal depths in the suture region between the two lithospheric domains (Sections 3.1 and 4.1.2).

Seismicity in the models is sensitive to multiple physical parameters, delineating a complex non-linear system. The different models highlight the importance of a sufficiently ductile lower crust and mantle wedge in allowing a realistic velocity and stress distribution (Figs. 4 and 5). They also show how significantly the temperature of the slab and its immediate surroundings affects crustal seismicity, particularly the seismic rate in the extensional regime and the seismic moment release in both the extensional and compressional regimes (Figs. 8 and 9). Such influence of slab and asthenospheric wedge temperatures on model seismicity, together with the significant observed seismic activity in both regimes in the orogen, suggest that the deep structure of the Northern Apennines includes a significantly cold and negatively buoyant subducting slab and a distinctly hot mantle wedge. The lack of observed earthquakes in the mantle, produced in the models through slab bending (Figs. 4 and 7), suggests that the lithospheric mantle in the models is either not strong or not ductile enough. As an alternative explanation, the lithospheric mantle might be undergoing aseismic creep or slow fault slip without generating earthquakes. However, it is also possible that the regional seismic velocity models used to locate earthquake hypocenters systematically underestimate deep velocities and thus the hypocentral depths. If so, at least some of the lower crustal earthquakes recorded there and not reproduced in our simulations could indeed be located immediately below the Adriatic Moho, thus eliminating some of the discrepancies between model results and observations.

4.3. Implications of deeper processes affecting upper crustal seismicity

The significance of results and conclusions from our numerical study likely goes beyond the specific setting of the Northern Apennines. In fact, this study shows the importance of long-term, large-scale dynamics on determining short-term tectonic regimes and seismicity. It also shows the influence of deep temperatures, strength and stiffness on short-term tectonics. In particular, these parameters significantly affect the stress regime as well as the speed of tectonic loading in the various domains of a geodynamic system. They thus alter the spatial partitioning of earthquakes between different regions (Sections 3.3 to 3.5 and 4.2 and Figs. 8 and 9). The specific respone of the simulated system to changes in model parameters is complex and certainly depends on the details of the setup and rheological quantities. Nevertheless,there is no reason why a broadly similar setup representing another orogenic system dynamically driven by its own buoyancy structure, especially if via lithospheric delamination-retreat, would lack any sensitivity of short-term crustal tectonics to deep rheology and the resulting dynamics. Certainly, our models indicate that the possibility exists for interplay between rheological complexity and geometrical structure resulting in the crustal seismicity being highly sensitive to various physical and rheological features of deep material. Furthermore, the models suggest that tectonic loading in systems with complex fault networks can be spatially complex and therefore cannot be modeled using a simple boundary condition with uniform far-field relative displacements. It thus needs to be simulated at least partly self-consistently and with the inclusion of realistic driving forces and tectonic loading to be able to correctly reproduce the distribution, frequency, size and type of seismicity in different areas. Overall, both long- and short-term dynamics, and therefore the lower crustal rheologies, deep thermal structure and material parameters that affect them, are needed for a complete physics-based seismic hazard assessment of a region with complex loading conditions resulting from tectonic forces. This importance of realistic tectonic loading and complex rheological structures on seismicity should be taken into account in physics-based seismic simulations (e.g., Dieterich and Richards-Dinger, 2010).

These results also imply that evidence of certain tectonic regimes, in terms of surface deformation and stress orientation, can be used to constrain the rheological structure and driving forces that cause them. Conversely, given a realistic rheological-structural model of the crust, present-day observations can be extended to also use seismicity to point towards plausible lithospheric and asthenospheric rheologies and long-term flow patterns and important parameters such as mantle viscosity and material strength.

4.4. Limitations

This study shows that STM modeling can partly reproduce the observed seismically active tectonic regimes in a very complex system in which deformation is driven by buoyancy forces. This methodology can be applied to a variety of tectonic regimes in complex and diverse geodynamic settings. However, the current limitations of our numerical methodology need to be considered. Two major limitations are the purely slip rate–dependent friction and the coarse temporal resolution. Both of these have been recently addressed in a newer version of the numerical code, which is yet to be tested on large-scale models (Herrendörfer et al., 2018). Short-term model characteristics such as the duration of events as well as their specific frequency and size may thus be affected, but the long-term stress regimes and resulting large-scale distribution of events in the extensional and compressional domains are likely to be robust. Another major limitation is the 2D model geometry. This allows a relatively simple model setup procedure and short run times, but implies the assumption of lateral homogeneity of the system, which is unrealistic for a real-world orogen.

5. Conclusions

We investigated the link between the lithospheric-scale geodynamic deformation and the relatively short-term tectonics and seismicity in the Northern Apennines orogen. We use seismo-thermo-mechanical numerical modeling and compare our results with earthquake catalogs and GPS observations. Results show that a large-scale dynamic regime driven by negative slab buoyancy can broadly reproduce the distinct, coupled extensional and compressional tectonic regimes of the Northern Apennines, in terms of both stress orientations and velocities. The latter, in particular, exhibit the coupling of uplift with extension

and subsidence with compression that characterizes the region. Nevertheless, discrepancies remain between modeled and observed vertical surface velocities. This misfit could indicate spatial and temporal changes in orogen behavior, deviating somewhat from the modeled geodynamic mechanism. However, it could also be due at least partly to shallow crustal processes.

The models can reproduce realistic tectonic regimes thanks to a highly ductile lower crust rheology (here, wet quartzite) and high temperatures. The resulting highly ductile lower crustal material, together with the hot asthenospheric wedge, protrudes upward and northwards as the negatively buoyant slab sinks and retreats. This flow of material produces uplift and extension in the overlying mountain range and decouples the upper crust from the lithospheric mantle, which delaminates. Ahead of the protruding material, where the upper crust is still coupled to the lithospheric mantle, subsidence and compression are produced. Our models thus indicate that thermally- and rheologically-controlled slab sinking and retreat and lower crustal deformation are needed to achieve the observed tectonic configuration of the orogen, as previously suggested by Chiarabba et al. (2014); Benoit et al. (2011).

The two tectonic regimes reproduced in the models generate seismicity, which is affected quite strongly in its cumulative released moment and spatial distribution by unexpected parameters. Slab pull controls critically both the distribution of seismic activity in the two tectonic regimes of the orogen. A colder and thus more negatively buoyant slab increases slab pull and thus the intensity of tectonic loading and the deformation and seismicity of the upper crust. Other material properties, such as slab stiffness and the strength of both bulk rock and faults, also influence the specific features of crustal seismicity. The shear modulus of the slab has a variable but broadly dampening effect on the release of seismic moment in the crust, which reflects the delamination-retreat mechanism that drives tectonics in the model. These results highlight the influence of the physical properties of deep material, at lithospheric mantle depths, on upper crustal seismicity. This influence is comparable with that of rock and fault strength, whose effect on earthquake ruptures is more direct and of widely acknowledged importance. This implies that research aiming to simulate the spatio-temporal distribution of earthquakes in complex fault systems should consider realistic forcing and rheologies to obtain appropriate loading of faults and surrounding rocks.

The success of STM modeling in reproducing some major features of the regional tectonics of the Northern Apennines and in describing the complex influence of key physical parameters on such tectonics paves the way for future applications, which could ultimately contribute to improved regional seismic hazard assessments.

Declaration of Competing Interest

The authors declare that they have no known competing financial interests or personal relationships that could have appeared to influence the work reported in this paper.

Acknowledgments

For constructive comments we thank the STM group at ETH Zürich and Prof. Liviu Matenco at Utrecht University. We thank Prof. Laurent Jolivet and an anonymous reviewer for their constructive reviews that improved the manuscript. We also thank Dr. Rob Govers, PhD supervisor of the first author of this paper, for allowing him to complete this work while working at Utrecht University.

This study is based on research work that was undertaken by first author Mario D'Acquisto at ETH Zürich as part of his degree of MSc in Earth Sciences and which resulted in a dissertation, available from the ETH Library.

Numerical simulations were run on the Euler cluster of ETH Zürich and on the Piz Daint supercomputer of the Swiss National Supercomputing Centre (Centro Svizzero di Calcolo Scientifico, CSCS) under project number s741. The simulations run on Euler used a computing node each, consisting of two 12-core Intel Xeon processor, while those run on Piz Daint shared Cray XC50 nodes, containing a 12-core Intel Xeon processor each.

The model executable, input files and model output used for figures in this article are available in a repository at doi:https://doi.org/10.5281/zenodo.3779998.

This study was partly funded by the SNSF SINERGIA project Swiss-AlpArray.

Appendix A. Appendices A–C

Supplementary data to this article can be found online at https://doi.org/10.1016/j.tecto.2020.228481.

References

Allmann, B.P., Shearer, P.M., 2009. Global variations of stress drop for moderate to large earthquakes. J. Geophys. Res. 114, B01310. https://doi.org/10.1029/2008JB005821.

Amitrano, D., 2003. Brittle-ductile transition and associated seismicity: Experimental and numerical studies and relationship with the b value. J. Geophys. Res. 108.

Ampuero, J.P., Ben-Zion, Y., 2008. Cracks, pulses and macroscopic asymmetry of dynamic rupture on a bimaterial interface with velocity-weakening friction. Geophys. J. Int. 173, 674–692. https://doi.org/10.1111/j.1365-246X.2008.03736.x.

Andrić, N., Vogt, K., Matenco, L., Cvetković, V., Cloetingh, S., Gerya, T., 2018. Variability of orogenic magmatism during Mediterranean-style continental collisions: a numerical modelling approach. Gondwana Res. 56, 119–134. https://doi.org/10.1016/j.gr.2017.12.007.

Balázs, A., Burov, E., Matenco, L., Vogt, K., Francois, T., Cloetingh, S., 2017. Symmetry during the syn- and post-rift evolution of extensional back-arc basins: the role of inherited orogenic structures. Earth Planet. Sci. Lett. 462, 86–98. https://doi.org/10.1016/j.epsl.2017.01.015.

Balestrieri, M.L., Bernet, M., Brandon, M.T., Picotti, V., Reiners, P., Zattin, M., 2003. Pliocene and Pleistocene exhumation and uplift of two key areas of the Northern Apennines. Quat. Int. 101–102, 67–73. https://doi.org/10.1016/S1040-6182(02)00089-7.

Bartolini, C., 2003. When did the Northern Apennine become a mountain chain? Quat. Int. 101–102, 75–80. https://doi.org/10.1016/S1040-6182(02)00090-3.

Bennett, R.A., Serpelloni, E., Hreinsdóttir, S., Brandon, M.T., Buble, G., Basic, T., Casale, G., Cavaliere, A., Anzidei, M., Marjonovic, M., Minelli, G., Molli, G., Montanari, A., 2012. Syn-convergent extension observed using the RETREAT GPS network, northern Apennines, Italy: NORTHERN APENNINES DEFORMATION. J. Geophys. Res. 117. https://doi.org/10.1029/2011JB008744.

Benoit, M.H., Torpey, M., Liszewski, K., Levin, V., Park, J., 2011. P and S wave upper mantle seismic velocity structure beneath the northern Apennines: New evidence for the end of subduction. Geochem. Geophys. Geosyst. 12. https://doi.org/10.1029/2010GC003428.

Bertotti, G., Mosca, P., Juez, J., Polino, R., Dunai, T., 2006. Oligocene to Present kilometres scale subsidence and exhumation of the Ligurian Alps and the Tertiary Piedmont Basin (NW Italy) revealed by apatite (U–Th)/He thermochronology: Correlation with regional tectonics. Terra Nova 18, 18–25. https://doi.org/10.1111/j.1365-3121.2005.00655.x. _eprint. https://onlinelibrary.wiley.com/doi/pdf/10.1111/j.1365-3121.2005.00655.x.

Bianchi, I., Park, J., Piana Agostinetti, N., Levin, V., 2010. Mapping seismic anisotropy using harmonic decomposition of receiver functions: an application to Northern Apennines, Italy. J. Geophys. Res. 115, 1–14. https://doi.org/10.1029/2009JB007061.

Bilek, S.L., Conrad, C.P., Lithgow-Bertelloni, C., 2005. Slab pull, slab weakening, and their relation to deep intra-slab seismicity: SLAB PULL AND SLAB WEAKENING. Geophys. Res. Lett. 32https://doi.org/10.1029/2005GL022922. n/a–n/a.

Blaser, L., Krüger, F., Ohrnberger, M., Scherbaum, F., 2010. Scaling relations of earthquake source parameter estimates with special focus on subduction environmentScaling relations of earthquake source Parameter estimates with focus on subduction environment. Bull. Seismol. Soc. Am. 100, 2914–2926. https://doi.org/10.1785/0120100111.

Carminati, E., Doglioni, C., Scrocca, D., 2003. Apennines subduction-related subsidence of Venice (Italy). Geophys. Res. Lett. 30. https://doi.org/10.1029/2003GL017001.

Carminati, E., Lustrino, M., Doglioni, C., 2012. Geodynamic evolution of the central and western Mediterranean: Tectonics vs. igneous petrology constraints. Tectonophysics 579, 173–192. https://doi.org/10.1016/j.tecto.2012.01.026.

Cerrina Feroni, A., Ottria, G., Martinelli, P., Martelli, L., 2002. Carta Geologico-Strutturale dell'Appennino Emiliano-Romagnolo. CNR, Florence, Italy (in Italian).

Cheloni, D., Giuliani, R., D'Agostino, N., Mattone, M., Bonano, M., Fornaro, G., Lanari, R., Reale, D., Atzori, S., 2016. New insights into fault activation and stress transfer between en echelon thrusts: The 2012 Emilia, Northern Italy, earthquake sequence. J. Geophys. Res. 121, 4742–4766. https://doi.org/10.1002/2016JB012823.

Chiarabba, C., De Gori, P., 2016. The seismogenic thickness in Italy: constraints on

potential magnitude and seismic hazard. Terra Nova 28, 402–408.
Chiarabba, C., Jovane, L., Di Stefano, R., 2005. A new view of Italian seismicity using 20 years of instrumental recordings. Tectonophysics 395, 251–268. https://doi.org/10.1016/j.tecto.2004.09.013.
Chiarabba, C., Giacomuzzi, G., Bianchi, I., Agostinetti, N.P., Park, J., 2014. From underplating to delamination-retreat in the northern Apennines. Earth Planet. Sci. Lett. 403, 108–116. https://doi.org/10.1016/j.epsl.2014.06.041.
Chiaraluce, L., Barchi, M., Collettini, C., Mirabella, F., Pucci, S., 2005. Connecting seismically active normal faults with Quaternary geological structures in a complex extensional environment: The Colfiorito 1997 case history (northern Apennines, Italy). Tectonics 24, TC1002. https://doi.org/10.1029/2004TC001627.
Clauser, C., Huenges, E., 1995. Thermal conductivity of rocks and minerals. In: Rock physics and phase relations: a handbook of physical constants. 3. pp. 105–126.
Cochard, A., Madariaga, R., 1994. Dynamic faulting under rate-dependent friction. Pure Appl. Geophys. 142, 419–445. https://doi.org/10.1007/BF00876049.
Collettini, C., De Paola, N., Holdsworth, R.E., Barchi, M.R., 2006. The development and behaviour of low-angle normal faults during Cenozoic asymmetric extension in the Northern Apennines, Italy. J. Struct. Geol. 28, 333–352.
Crameri, F., Schmeling, H., Golabek, G., Duretz, T., Orendt, R., Buiter, S., May, D., Kaus, B., Gerya, T., Tackley, P., 2012. A comparison of numerical surface topography calculations in geodynamic modelling: an evaluation of the sticky airmethod. Geophys. J. Int. 189, 38–54.
Dal Zilio, L., van Dinther, Y., Gerya, T.V., Pranger, C.C., 2018. Seismic behaviour of mountain belts controlled by plate convergence rate. Earth Planet. Sci. Lett. 482, 81–92. https://doi.org/10.1016/j.epsl.2017.10.053.
Devoti, R., Riguzzi, F., Cuffaro, M., Doglioni, C., 2008. New GPS constraints on the kinematics of the Apennines subduction. Earth Planet. Sci. Lett. 273, 163–174. https://doi.org/10.1016/j.epsl.2008.06.031.
Devoti, R., Esposito, A., Pietrantonio, G., Pisani, A.R., Riguzzi, F., 2011. Evidence of large scale deformation patterns from GPS data in the Italian subduction boundary. Earth Planet. Sci. Lett. 311, 230–241. https://doi.org/10.1016/j.epsl.2011.09.034.
Di Stefano, R., Kissling, E., Chiarabba, C., Amato, A., Giardini, D., 2009. Shallow subduction beneath Italy: Three-dimensional images of the Adriatic-European-Tyrrhenian lithosphere system based on high-quality P wave arrival times. J. Geophys. Res. 114, 1–17. https://doi.org/10.1029/2008JB005641.
Di Toro, G., Han, R., Hirose, T., De Paola, N., Nielsen, S., Mizoguchi, K., Ferri, F., Cocco, M., Shimamoto, T., 2011a. Fault lubrication during earthquakes. Nature 471, 494–498. https://doi.org/10.1038/nature09838.
Di Toro, G., Han, R., Hirose, T., De Paola, N., Nielsen, S., Mizoguchi, K., Ferri, F., Cocco, M., Shimamoto, T., 2011b. Fault lubrication during earthquakes. Nature 471, 494.
Dieterich, J.H., Richards-Dinger, K.B., 2010. Earthquake Recurrence in simulated Fault Systems. In: Savage, M.K., Rhoades, D.A., Smith, E.G.C., Gerstenberger, M.C., Vere-Jones, D. (Eds.), Seismogenesis and Earthquake Forecasting: The Frank Evison Volume II. Springer Basel, Basel, pp. 233–250. https://doi.org/10.1007/978-3-0346-0500-7_15. Pageoph Topical Volumes.
van Dinther, Y., Gerya, T.V., Dalguer, L.A., Corbi, F., Funiciello, F., Mai, P.M., 2013a. The seismic cycle at subduction thrusts: 2. Dynamic implications of geodynamic simulations validated with laboratory models. J. Geophys. Res. 118, 1502–1525. https://doi.org/10.1029/2012JB009479.
van Dinther, Y., Gerya, T.V., Dalguer, L.A., Mai, P.M., Morra, G., Giardini, D., 2013b. The seismic cycle at subduction thrusts: Insights from seismo-thermo-mechanical models. J. Geophys. Res. 118, 6183–6202. https://doi.org/10.1002/2013JB010380.
Ersoy, E.Y., Palmer, M.R., 2013. Eocene-Quaternary magmatic activity in the Aegean: Implications for mantle metasomatism and magma genesis in an evolving orogeny. Lithos 180–181, 5–24. https://doi.org/10.1016/j.lithos.2013.06.007.
Faccenda, M., Minelli, G., Gerya, T.V., 2009. Coupled and decoupled regimes of continental collision: Numerical modeling. Earth Planet. Sci. Lett. 278, 337–349. https://doi.org/10.1016/j.epsl.2008.12.021.
Faccenna, C., Mattei, M., Funiciello, R., Jolivet, L., 1997. Styles of back-arc extension in the Central Mediterranean. Terra Nova 9, 126–130. https://doi.org/10.1046/j.1365-3121.1997.d01-12.x. _eprint. https://onlinelibrary.wiley.com/doi/pdf/10.1046/j.1365-3121.1997.d01-12.x.
Faccenna, C., Becker, T.W., Lucente, F.P., Jolivet, L., Rossetti, F., 2001. History of subduction and back arc extension in the Central Mediterranean. Geophys. J. Int. 145, 809–820. https://doi.org/10.1046/j.0956-540x.2001.01435.x.
Faccenna, C., Becker, T.W., Jolivet, L., Keskin, M., 2013. Mantle convection in the Middle East: Reconciling Afar upwelling, Arabia indentation and Aegean trench rollback. Earth Planet. Sci. Lett. 375, 254–269. https://doi.org/10.1016/j.epsl.2013.05.043.
Faccenna, C., Becker, T.W., Auer, L., Billi, A., Boschi, L., Brun, J.P., Capitanio, F.A., Funiciello, F., Horvàth, F., Jolivet, L., Piromallo, C., Royden, L., Rossetti, F., Serpelloni, E., 2014a. Mantle dynamics in the Mediterranean. Rev. Geophys. 52, 283–332. https://doi.org/10.1002/2013RG000444. _eprint. https://onlinelibrary.wiley.com/doi/pdf/10.1002/2013RG000444.
Faccenna, C., Becker, T.W., Miller, M.S., Serpelloni, E., Willett, S.D., 2014b. Isostasy, dynamic topography, and the elevation of the Apennines of Italy. Earth Planet. Sci. Lett. 407, 163–174. https://doi.org/10.1016/j.epsl.2014.09.027.
Funiciello, F., Moroni, M., Piromallo, C., Faccenna, C., Cenedese, A., Bui, H.A., 2006. Mapping mantle flow during retreating subduction: Laboratory models analyzed by feature tracking. J. Geophys. Res. 111. https://doi.org/10.1029/2005JB003792. _eprint. https://onlinelibrary.wiley.com/doi/pdf/10.1029/2005JB003792.
Gerya, T.V., Yuen, D.A., 2007. Robust characteristics method for modelling multiphase visco-elasto-plastic thermo-mechanical problems. Phys. Earth Planet. Inter. 163, 83–105. https://doi.org/10.1016/j.pepi.2007.04.015.
Heidbach, O., Rajabi, M., Reiter, K., Ziegler, M., 2016. World Stress Map 2016. https://doi.org/10.5880/WSM.2016.002.
Herrendörfer, R., Gerya, T., van Dinther, Y., 2018. An invariant rate- and state-dependent friction formulation for viscoeastoplastic earthquake cycle simulations. J. Geophys. Res. 123, 5018–5051. https://doi.org/10.1029/2017JB015225.
Heuret, A., Lallemand, S., Funiciello, F., Piromallo, C., Faccenna, C., 2011. Physical characteristics of subduction interface type seismogenic zones revisited: SUBDUCTION-TYPE SEISMOGENIC ZONES. Geochem. Geophys. Geosyst. 12https://doi.org/10.1029/2010GC003230. n/a–n/a.
van Hinsbergen, D.J.J., Vissers, R.L.M., Spakman, W., 2014. Origin and consequences of western Mediterranean subduction, rollback, and slab segmentation. Tectonics 33, 393–419. https://doi.org/10.1002/2013TC003349. _eprint. https://onlinelibrary.wiley.com/doi/pdf/10.1002/2013TC003349.
van Hinsbergen, D.J., Torsvik, T.H., Schmid, S.M., Maţenco, L.C., Maffione, M., Vissers, R.L., Gürer, D., Spakman, W., 2020. Orogenic architecture of the Mediterranean region and kinematic reconstruction of its tectonic evolution since the Triassic. Gondwana Res. 81, 79–229. https://doi.org/10.1016/j.gr.2019.07.009.
Horváth, F., Musitz, B., Balázs, A., Végh, A., Uhrin, A., Nádor, A., Koroknai, B., Pap, N., Tóth, T., Wórum, G., 2015. Evolution of the Pannonian basin and its geothermal resources. Geothermics 53, 328–352. https://doi.org/10.1016/j.geothermics.2014.07.009.
Jolivet, L., Brun, J.P., 2010. Cenozoic geodynamic evolution of the Aegean. Int. J. Earth Sci. 99, 109–138. https://doi.org/10.1007/s00531-008-0366-4.
Jolivet, L., Faccenna, C., 2000. Mediterranean extension and the Africa-Eurasia collision. Tectonics 19, 1095–1106. https://doi.org/10.1029/2000TC900018. _eprint. https://onlinelibrary.wiley.com/doi/pdf/10.1029/2000TC900018.
Jolivet, L., Faccenna, C., Huet, B., Labrousse, L., Le Pourhiet, L., Lacombe, O., Lecomte, E., Burov, E., Denèle, Y., Brun, J.P., Philippon, M., Paul, A., Salaün, G., Karabulut, H., Piromallo, C., Monié, P., Gueydan, F., Okay, A.I., Oberhänsli, R., Pourteau, A., Augier, R., Gadenne, L., Driussi, O., 2013. Aegean tectonics: Strain localisation, slab tearing and trench retreat. Tectonophysics 597-598, 1–33. https://doi.org/10.1016/j.tecto.2012.06.011.
Jolivet, L., Romagny, A., Gorini, C., Maillard, A., Thinon, I., Couëffé, R., Ducoux, M., Séranne, M., 2020. Fast dismantling of a mountain belt by mantle flow: Late-orogenic evolution of Pyrenees and Liguro-Provençal rifting. Tectonophysics 776, 228312. https://doi.org/10.1016/j.tecto.2019.228312.
Katsura, T., Yoneda, A., Yamazaki, D., Yoshino, T., Ito, E., 2010. Adiabatic temperature profile in the mantle. Phys. Earth Planet. Inter. 183, 212–218. https://doi.org/10.1016/j.pepi.2010.07.001.
Király, Á., Faccenna, C., Funiciello, F., 2018. Subduction zones Interaction around the Adria Microplate and the Origin of the Apenninic Arc. Tectonics 37, 3941–3953. https://doi.org/10.1029/2018TC005211. _eprint. https://onlinelibrary.wiley.com/doi/pdf/10.1029/2018TC005211.
Konstantinou, K., 2017. Accurate relocation of seismicity along the North Aegean Trough and its relation to active tectonics. Tectonophysics 717, 372–382. https://doi.org/10.1016/j.tecto.2017.08.021.
Kruckenberg, S.C., Vanderhaeghe, O., Ferré, E.C., Teyssier, C., Whitney, D.L., 2011. Flow of partially molten crust and the internal dynamics of a migmatite dome, Naxos, Greece. Tectonics 30https://doi.org/10.1029/2010TC002751. _eprint. https://onlinelibrary.wiley.com/doi/pdf/10.1029/2010TC002751.
Le Breton, E., Handy, M.R., Molli, G., Ustaszewski, K., 2017. Post-20 Ma motion of the Adriatic Plate: New Constraints from surrounding orogens and implications for crust-mantle decoupling. Tectonics 36, 3135–3154. https://doi.org/10.1002/2016TC004443.
Leever, K.A., Matenco, L., Bertotti, G., Cloetingh, S., Drijkoningen, G.G., 2006. Late orogenic vertical movements in the Carpathian Bend Zone – seismic constraints on the transition zone from orogen to foredeep. Basin Res. 18, 521–545. https://doi.org/10.1111/j.1365-2117.2006.00306.x. _eprint. https://onlinelibrary.wiley.com/doi/pdf/10.1111/j.1365-2117.2006.00306.x.
Mantovani, E., Viti, M., Babbucci, D., Tamburelli, C., Cenni, N., Baglione, M., D'Intinosante, V., 2015a. Present tectonic setting and spatio-temporal distribution of seismicity in the apennine belt. Int. J. Geosci. 6, 429. https://doi.org/10.4236/ijg.2015.64034.
Mantovani, E., Viti, M., Cenni, N., Babbucci, D., Tamburelli, C., 2015b. Present velocity field in the Italian Region by GPS data: geodynamic/tectonic implications. Int. J. Geosci. 06, 1285. https://doi.org/10.4236/ijg.2015.612103.
Menant, A., Jolivet, L., Vrielynck, B., 2016. Kinematic reconstructions and magmatic evolution illuminating crustal and mantle dynamics of the eastern Mediterranean region since the late Cretaceous. Tectonophysics 675, 103–140. https://doi.org/10.1016/j.tecto.2016.03.007.
Métois, M., D'Agostino, N., Avallone, A., Chamot-Rooke, N., Rabaute, A., Duni, L., Kuka, N., Koci, R., Georgiev, I., 2015. Insights on continental collisional processes from GPS data: Dynamics of the peri-Adriatic belts. J. Geophys. Res. 120, 8701–8719. https://doi.org/10.1002/2015JB012023. _eprint. https://onlinelibrary.wiley.com/doi/pdf/10.1002/2015JB012023.
Molli, G., 2008. Northern Apennine–Corsica orogenic system: an updated overview. Geol. Soc. Lond., Spec. Publ. 298, 413–442. https://doi.org/10.1144/SP298.19.
Molli, G., Crispini, L., Malusà, M.G., Mosca, P., Piana, F., Federico, L., 2010. Geology of the Western Alps-Northern Apennine junction area: a regional review. J. Virtual Explor. 36. https://doi.org/10.3809/jvirtex.2009.00215.
Panza, G.F., Chimera, G., Pontevivo, A., Aoudia, A., Raykova, R., 2003. The lithosphere-asthenosphere: Italy and surroundings. Episodes 26, 169–174.
Panza, G.F., Peccerillo, A., Aoudia, A., Farina, B., 2007. Geophysical and petrological modelling of the structure and composition of the crust and upper mantle in complex geodynamic settings: The Tyrrhenian Sea and surroundings. Earth Sci. Rev. 80, 1–46. https://doi.org/10.1016/j.earscirev.2006.08.004.
Pasquale, V., Chiozzi, P., Verdoya, M., 2010. Tectonothermal processes and mechanical strength in a recent orogenic belt: Northern Apennines. J. Geophys. Res. 115, 1–17. https://doi.org/10.1029/2009JB006631.

Pasquale, V., Chiozzi, P., Verdoya, M., 2013. Evidence for thermal convection in the deep carbonate aquifer of the eastern sector of the Po Plain, Italy. Tectonophysics 594, 1–12. https://doi.org/10.1016/j.tecto.2013.03.011.

Patacca, E., Sartori, R., Scandone, P., 1990. Tyrrhenian Basin and Apenninic arcs; kinematic relations since late Tortonian times. In: Memorie Della Societa Geologica Italiana, Societa Geologica Italiana, Rome, pp. 425–451.

Piccinini, D., Piana Agostinetti, N., Saccorotti, G., Fiaschi, A., Matassoni, L., Morelli, M., 2014. Orogen-parallel variability in 3D seismicity distribution, Northern Apennines (Italy): evidence for a slab tear fault? J. Geodyn. 82, 110–117. https://doi.org/10.1016/j.jog.2014.09.005.

Picotti, V., Pazzaglia, F.J., 2008. A new active tectonic model for the construction of the Northern Apennines mountain front near Bologna (Italy). J. Geophys. Res. 113, 1–24. https://doi.org/10.1029/2007JB005307.

Pondrelli, S., Salimbeni, S., Ekström, G., Morelli, A., Gasperini, P., Vannucci, G., 2006. The Italian CMT dataset from 1977 to the present. Phys. Earth Planet. Inter. 159, 286–303. https://doi.org/10.1016/j.pepi.2006.07.008.

Ranalli, G., 1995. Rheology of the Earth. Springer Science & Business Media.

Rovida, A., Locati, M., Camassi, R., Lolli, B., Gasperini, P., 2016. CPTI15, the 2015 version of the Parametric Catalogue of Italian Earthquakes. Istituto Nazionale di Geofisica e Vulcanologiahttps://doi.org/10.6092/INGV.IT-CPTI15.

Ruff, L., Kanamori, H., 1980. Seismicity and the subduction process. Phys. Earth Planet. Inter. 23, 240–252. https://doi.org/10.1016/0031-9201(80)90117-X.

Scholz, C.H., 2015. On the stress dependence of the earthquake b value. Geophys. Res. Lett. 42, 1399–1402.

Scognamiglio, L., Margheriti, L., Mele, F.M., Tinti, E., Bono, A., De Gori, P., Lauciani, V., Lucente, F.P., Mandiello, A.G., Marcocci, C., Mazza, S., Pintore, S., Quintiliani, M., 2012. The 2012 Pianura Padana Emiliana seimic sequence: Locations, moment tensors and magnitudes. Ann. Geophys. 55, 549–559. https://doi.org/10.4401/ag-6159.

Serpelloni, E., Faccenna, C., Spada, G., Dong, D., Williams, S.D.P., 2013. Vertical GPS ground motion rates in the Euro-Mediterranean region: New evidence of velocity gradients at different spatial scales along the Nubia-Eurasia plate boundary: GPS VERTICAL DEFORMATION IN EUROPE. J. Geophys. Res. 118, 6003–6024. https://doi.org/10.1002/2013JB010102.

Spada, M., Bianchi, I., Kissling, E., Agostinetti, N.P., Wiemer, S., 2013. Combining controlled-source seismology and receiver function information to derive 3-D moho topography for Italy. Geophys. J. Int. 194, 1050–1068. https://doi.org/10.1093/gji/ggt148.

Spakman, W., Chertova, M.V., van den Berg, A., van Hinsbergen, D.J.J., 2018. Puzzling features of western Mediterranean tectonics explained by slab dragging. Nat. Geosci. 11, 211–216. https://doi.org/10.1038/s41561-018-0066-z.

Thomson, S.N., Brandon, M.T., Reiners, P.W., Zattin, M., Isaacson, P.J., Balestrieri, M.L., 2010. Thermochronologic evidence for orogen-parallel variability in wedge kinematics during extending convergent orogenesis of the northern Apennines, Italy. Geol. Soc. Am. Bull. 122, 1160–1179. https://doi.org/10.1130/B26573.1.

Tizzani, P., Castaldo, R., Solaro, G., Pepe, S., Bonano, M., Casu, F., Manunta, M., Manzo, M., Pepe, A., Samsonov, S., Lanari, R., Sansosti, E., 2013. New insights into the 2012 Emilia (Italy) seismic sequence through advanced numerical modeling of ground deformation InSAR measurements. Geophys. Res. Lett. 40, 1971–1977. https://doi.org/10.1002/grl.50290.

Ventura, G., Cinti, F.R., Luccio, F.D., Pino, N.A., 2007. Mantle wedge dynamics versus crustal seismicity in the Apennines (Italy). Geochem. Geophys. Geosyst. 8https://doi.org/10.1029/2006GC001421. _eprint. https://onlinelibrary.wiley.com/doi/pdf/10.1029/2006GC001421.

Vergés, J., Fernàndez, M., 2012. Tethys–Atlantic interaction along the Iberia–Africa plate boundary: The Betic–Rif orogenic system. Tectonophysics 579, 144–172. https://doi.org/10.1016/j.tecto.2012.08.032.